Pervasive melt percolation reactions in ultra-depleted refractory harzburgites at the Mid-Atlantic Ridge, 15° 20' N : ODP Hole 1274A.

M. Seyler[1], J.-P. Lorand[1], H.J.B. Dick[2], M. Drouin[3]

[1]Museum National d'Histoire Naturelle, CNRS UMR7160 Minéralogie – Pétrologie, 61 rue Buffon, 75005 Paris, France

[2]Woods Hole Oceanographic Institution, Woods Hole, MA 02543, USA

[3]Laboratoire de Tectonophysique, CNRS UMR 5568, Université de Montpellier 2, Place Eugène Bataillon, 34095 Montpellier Cedex 05, France

Corresponding author:

Monique Seyler
Université Lille1, UFR Sciences de la Terre
Bât. SN5
59655 Villeneuve d'Ascq cedex
FRANCE
Telephone: +(33) 3 20 43 45 69
Email: Monique.Seyler@univ-lille1.fr

Abstract

ODP Leg 209 Site 1274 mantle peridotites are highly refractory in terms of lack of residual clinopyroxene, olivine Mg# (up to 0.92) and spinel Cr# (~0.5), suggesting high degree of partial melting (>20%). Detailed studies of their microstructures show that they have extensively reacted with a pervading intergranular melt prior to cooling in the lithosphere, leading to crystallization of olivine, clinopyroxene and spinel at the expense of orthopyroxene. The least reacted harzburgites are too rich in orthopyroxene to be simple residues of low-pressure (spinel field) partial melting. Cu-rich sulfides that precipitated with the clinopyroxenes indicate that the intergranular melt was generated by no more than 12% melting of a MORB mantle or by more extensive melting of a clinopyroxene-rich lithology. Rare olivine-rich lherzolitic domains, characterized by relics of coarse clinopyroxenes intergrown with magmatic sulfides, support the second interpretation. Further, coarse and intergranular clinopyroxenes are highly depleted in REE, Zr and Ti. A two-stage partial melting/melt-rock reaction history is proposed, in which initial mantle underwent depletion and refertilization after an earlier high pressure (garnet field) melting event before upwelling and remelting beneath the present-day ridge. The ultra-depleted compositions were acquired through melt re-equilibration with residual harzburgites.

Introduction

Abyssal peridotites are widely considered as complementary residues of mid-oceanic ridge basalts (MORBs) after variable degree of adiabiatic melting resulting from decompression of the mantle beneath spreading ridges. In this view, their structure, texture and composition must provide valuable information on melting and melt extraction processes and source composition. Current models assume that melts segregate from their sources after a very few percent melting and are rapidly extracted from the surrounding mantle to be transferred into high-porosity channels, where they are transported to the surface with no chemical interaction with the shallow mantle (Kelemen et al. 1997). Strongly depleted light to heavy rare earth element ratios (LREE/HREE) in residual clinopyroxene (Cpx) are indeed indisputable evidence for near-fractional melt extraction beneath spreading ridges (Johnson et al. 1990; Johnson and Dick 1992). On the other hand, it is argued that the last melt fractions produced by low-P partial melting of depleted peridotites may travel by diffuse porous flow, leading to extensive melt-rock reaction and peridotite refertilization in the shallow mantle (Kelemen et al. 1997; Asimow 1999; Dijkstra et al. 2003). Recently, it was recognized that a small proportion of Cpx in abyssal peridotites is not residual, but crystallized from melt as the partially molten mantle

enters into the conductive thermal layer (Seyler et al. 2001; Hellebrand et al. 2002; Brunelli et al. 2006). This observation supports the idea of refertilization of the fractional melting residues by basaltic melt, which was first suggested by Elthon (1992). Reactive porous flow and refertilization are two important processes that are potentially able to deeply modify textures, mineral modes and chemical compositions of residual peridotites. Melt-rock interaction and refertilization were principally studied in plagioclase-bearing peridotites, in which feldspar-bearing veins and strong chemical gradients make these reactions immediately recognizable. In contrast, coarse-grained, plagioclase-free spinel peridotites show no obvious evidence of these reactions, because they theoretically cool at a greater depth. At a temperature close to the peridotite solidus and condition of low-strain deformation, residual and igneous minerals tend to textural and chemical equilibria. Serpentinization will then tend to blur or destroy any fragile evidence of reaction. As a consequence, description of reactional textures in abyssal peridotites is very few and little is known about the nature of reactions really involved in these processes. Hence, the extent of the reactions and the magnitude of the compositional changes they induce are poorly evaluated.

Ocean Drilling Program Leg 209 Site 1274 mantle peridotites appear to be most suitable to study these two aspects. They experienced a relatively low degree of serpentinization and textures show greater extent of diffuse melt-rock reaction than commonly observed in most abyssal peridotites. In this paper we describe in detail a variety of these high-T microstructures, which are believed to result from pervasive melt-rock reaction in partially molten peridotites. Petrographic observation coupled with in situ mineral chemistry allow us to investigate the nature and conditions of melt-rock reactions and to constrain some aspects of the melting history of the peridotites. Fe-Ni-Cu sulfides of magmatic origin have been studied in addition to major minerals. These base metal sulfides are important petrogenetic indicators of partial melting degree and melt-rock interactions, because they concentrate chalcophile trace elements (S, Cu) that partition very similarly to CaO and Al_2O_3 (Lorand 1988, 1991; Luguet et al. 2003).

Geological setting

The region of the Mid-Atlantic Ridge (MAR) extending across the 15°20'N Fracture Zone (FZ) has been the focus of numerous geophysical, dredging and submersible surveys, and was recently drilled at eight sites during Leg 209 of the Ocean Drilling Program (Escartin and Cannat 1999; Fujiwara et al. 2003; Kelemen et al. 2004, and review therein). In this region, basaltic crust is thin and discontinuous and mantle peridotites with gabbroic intrusions crop out nearly continuously on both sides of the rift valley from 14°40'N to 15°40'N. The overall

amount of gabbroic rocks is estimated to be 20%-40%, a proportion that would correspond to 5 km of " normal " oceanic crust (Kelemen 2003). Two gravity lows, centered at ~14°N and ~16°N, are interpreted as centers of magmatic segments where thick igneous crust accreted. Whereas the peridotites appear to have undergone an unusually high degree of melting (Bonatti et al. 1992; Cannat et al. 1992, 1997), the basalt compositions evolve from enriched-type MORBs in the 14°N region to normal-type MORBs in the 16°N region (Dosso et al. 1991, 1993).

ODP Leg 209, Site 1274, located 31 km north (15°65'N – 46°68'W) of the NW intersection of the MAR with the 15°20'N FZ (Fig. 1), has drilled into 156 m of mantle peridotite, with 35% recovery. Cores recovered are mainly residual peridotite, with a few m-scale gabbroic intrusions, and a large proportion of dunites (77% harzburgite; 20% dunite; 3% gabbros). Site 1274 peridotites contain the smallest proportion of gabbros with respect to other Leg 209 sites (Fig. 1). Thick fault gouge forms about 7% of the recovered cores, in the lower part of the hole, between ~95 mbsf and ~145 mbsf. Site 1274 peridotites are less serpentinized and weathered (up to 35% of the original mantle preserved) than Sites 1268 and 1272 peridotites (> 99% serpentinization). In the three sites, the peridotite protolith is dominated by harzburgites varying in composition from orthopyroxene (Opx)-rich (28-30 vol% Opx) to Opx-poor (10 vol%) to dunites. Cpx content represents 1-2 vol% of the peridotites (visual estimation), with rare, local concentrations, up to 4 vol%. In a few places, a rough Opx layering can be observed, but in general, rocks have coarse granular textures lacking high-T foliation and lineation.

Sample selection and analytical methods

The studied sample set comprises thirty-six harzburgites, one Cpx-rich harzburgite and one dunite. Harzburgites were sampled away from dunite bands and gabbros (Table 1; Fig. 2a). Each sample consists of a 35 x 25 mm billet, 0.5 to 0.75 cm thick, in which 1 to 3 standard sized thin sections have been cut. Primary modal proportions of twelve samples were reconstructed, using relict primary phases and their pseudomorphs, by point counting (steps of 1/3 mm; ~6000 points per sample). Detailed textural observation and modes of fine-grained mineral intergrowths were completed by analyzing back scattered electron images. In addition, the twenty-five SEY samples were investigated in reflected light microscopy to indentify base metal sulfides (BMS); their modal abundances (two polished thin sections per sample) were determined using a procedure reported in detail by Lorand and Grégoire (2006). Mineral compositions were analyzed with a CAMECA SX-100 electron microprobe at the University of

Paris VI and at Woods Hole Oceanographic Institute. The accelerating voltage was 15 kV and beam current was 40 nA (15 nA for Na). A 2 μm beam size was used for all minerals, except a subset of pyroxenes, for which average compositions including exsolution lamellae were obtained with a defocused beam (10-15 μm). Selected Cpx were analyzed for REEs, Zr, Ti and Sr by secondary ion mass spectrometry, using an upgraded Cameca IMS-4f ion microprobe at the University of Montpellier and following procedures described in Bottazzi et al. (1994).

Analytical results

Modal compositions

Olivine (Ol) and Opx contents in the studied harzburgites vary from 70.3 to 84.1 vol% and 13.4 to 27.2 vol%, respectively (Table 2). Cpx content is in the 0.7-2.6 vol% range in the harzburgites, and is 4.7 vol% in the Cpx-rich harzburgite; this sample, very close to lherzolite in Streckeisen's classification (1976), is referenced as lherzolite herein. Spinel (Sp) is ubiquitous and may be abundant in some samples (0.5-1.3 vol%). The average composition of the eleven harzburgites/lherzolite is 76.5% Ol, 20.6% Opx, 2.1% Cpx and 0.7% Sp, in the average of the visually estimated composition of Hole 1274A harzburgites (Kelemen et al. 2004). No correlation was found between Cpx and Opx or Ol contents, and the lherzolite is especially poor in Opx.

BMS have been detected in 75% of the studied thin sections (Fig. 2b). Owing to the average degree of serpentinization, all the BMS assemblages except a few inclusions in the Opx described below, systematically display partial replacement of primary sulfides (pentlandite $Fe_4Ni_5S_8$ to $Fe_5Ni_4S_8$ (unpublished EMP data), chalcopyrite $CuFeS_2$, bornite Cu_5FeS_4) by native copper, Ni_3Fe alloys and/or magnetite, and occasionally by heazlewoodite Ni_3S_2 and secondary Cu-rich sulfides (digenite Cu_9S_5 and valleriite $CuFe_2S_3,Mg(OH)_2$). This alteration sequence is common to abyssal peridotites (Luguet et al. 2003). Serpentinization-related opaque minerals preserved the original shape of magmatic sulfide grains, i.e. polyhedral (not euhedral) blebs with generally concave inward grain boundaries. Only such grains were used for modal abundance estimates.

Site 1274 peridotites may be as BMS-rich as fertile mantle lherzolites (up to 0.1 vol%), despite their average harzburgitic modal compositions. However, BMS are heterogeneously distributed, being concentrated in the uppermost 25 m of Hole 1274A and in the deeper Ol-rich harzburgite SEY23, two zones that yielded only harzburgites (Fig. 2a,b). The highest BMS concentrations correspond to high (>0.1) Cpx/Opx modal ratios (SEY03; SEY04; SEY23) and the lowest to Opx-rich samples (>20% Opx). However, BMS are strongly heterogeneously

distributed at the hand-sample scale which generated strong random sectioning effects. For example, one thin section in SEY09 contains almost no BMS whereas the other is the second richest one (0.08 vol% BMS). The near-zero BMS content of samples from 40 to 145 mbsf is worthy of note, because it seems to correspond with the occurrence of numerous dunites (although there are sampling gaps in our studied sample set).

Microstructures and grain morphology

Cm-sized, rounded olivine domains are mosaics of 3-4 mm-sized grains. Gently curved to polygonal grain boundaries, with an occasional subgrain boundary, suggest recrystallization of very coarse primary crystals. Opx porphyroclasts are highly variable in grain shape and size. Coarse to very coarse (> 1-2 cm), equant Opx are occasionally broken with formation of wedge-shaped fractures (Fig. 3a) which affect only the Opx grains and not adjacent Ol and display no specific orientation. Opx grain boundaries commonly display cuspate embayments filled with secondary Ol, varying in size from a few μm to a few mm. In many instances, Ol sides in contact with reacted Opx have developed faceted crystal boundaries, which suggests growth from, or re-equilibration with, a melt film that was present at the Ol-Opx interface; in some cases, this melt film is interpreted to have left behind a stringer of Cpx. With increasing degree of dissolution, some Opx grains become ovoid and define a flow structure. More typically, strong dissolution results in the formation of anhedral, thin, elongate grains, interstial to Ol. Replacive Ol commonly penetrates Opx along cleavage planes (Fig. 3b). Extensive replacement of Opx by Ol results in the parceling of the original, very coarse grains into what appears in thin section as clusters of variously shaped (angular to rounded) Opx clasts within a matrix of newly crystallized Ol. Ends of Opx porphyroclasts are preferentially corroded or intergrown with Sp several mms long and a few 100 μm wide (Fig. 3c). These aggregates are interpreted as recrystallized Opx parcels cemented by Sp and minor Cpx. This secondary material is arranged along the crystallographic directions of the host mineral and likely results from the infiltration of melt which reacted with the Opx, then precipitated Sp±Cpx. This material steps out the Opx in between adjacent Ol grains (Fig. 3c); at these sites, Ol is resorbed into tiny grains poikilitically enclosed in Sp. A few samples show high strain deformation, with mosaics of very fine grained (20-50 μm) Ol replacing Opx along kink bands and grain boundaries. However, Opx dynamic recrystallization was not observed in any samples.

Cpx occurs in two major textural types. The first type characterizes the lherzolite sample, where coarse (up to 5 mm) Cpx grains, with large exsolution lamellae of Opx and occasional twinning, form diffuse, one crystal thick, discontinous veins (Fig. 4a); some partially replace

Opx (Fig. 4b). Crystal boundaries show large embayments filled with Ol (Fig. 4a), similar to those in Opx porphyroclasts. However, in contrast with Opx, these Cpx have poikiloblastic rims, associated with tiny grains of Sp, that enclose adjacent Ol or Opx (Fig. 4a) and can be followed over several mm (Fig. 4c). Both cores and rims display intergrowths with magmatic sulfides (Fig. 4c,d). The second Cpx texture type, ubiquitous in the lherzolite and all harzburgites, consists of smaller grains, up to 2 mm in size, with thin exsolution lamellae of Opx and rare twinning. They typically form selvages on Opx, with Opx-Cpx contacts characterized by strong Opx resorption: Opx display convex-out grain boundaries and tends to be poikilitically enclosed by Cpx (Fig. 4e). Cpx selvages show thin extensions between adjacent Ol grains, locally widen into small to medium-sized, intergranular Cpx. Late-stage Cpx also fills low-angle triple junctions, V-shaped fractures in Opx, and small cracks in the Ol matrix.

Sp is found with recrystallized Opx (described in Opx section) or associated with late-stage Cpx. Sp shapes range from anhedral to blocky, subhedral porphyroblasts up to 2 mm sized, that are often overgrown by a corona of Cpx in spatial continuity with the Cpx selvages. Pyroxenes and Sp commonly form two types of fine-grained symplectites representing 0.5-2% of harzburgite modes. One symplectite type (S1) consists of Cpx grains intergrown with skeletal Sp in ~40:60 volume proportions, respectively, with no Opx (Fig. 3d). It occupies the same textural sites as the discrete Cpx, with both occurrences grading into each other. In particular, it fills Ol or Ol-Opx triple junctions, and surrounds the ovoid Opx. Thin stringers of S1 may also be observed at the edges of coarse Cpx in the lherzolite. A second symplectite type (S2) contains Opx in addition to Cpx and Sp rods. It forms bulbous, myrmekite-like assemblage, ~200 μm across, at Opx-Ol interfaces, with convex side of Opx toward Ol (Fig. 3e) and Sp branching perpendicular to the adjacent Ol. Although separated by Sp, Opx in S2 symplectite is in optical continuity with the primary Opx grain.

The average size of BMS grains range between 100 x 50 and 200 x 100 μm, but larger grains (up to 500 x 300 μm in maximum dimensions) occur in the lherzolite. BMS are not randomly distributed at the thin section scale. Most BMS grain occur at Opx-Ol or Cpx-Opx grain boundaries. Except in SEY23, very few BMS are surrounded by Ol alone. BMS occur in sites of Opx consumption, either protruding into Opx margins in contact with secondary Ol (15%) or as disseminated blebs adjacent Cpx selvages (50%). Respectively 40% and 30% of about 300 counted grains of BMS share a grain boundary with an Opx or a Cpx crystal, whereas the latter two silicates account for only 20% and 2%, respectively, of harzburgite modes. In some cases, BMS are sealed at the Opx outer margins by a continuous poikiloblastic Cpx rims. Sulfide melts penetrated corrosion paths, thus creating secondary sulfide inclusion networks

within the Opx (Fig. 4f). Their BMS assemblages (pentlandite + chalcopyrite + bornite in unfractured, closed inclusions; abundant native Cu in fractured, open inclusions) provide evidence for Cu-rich sulfide parent melts. Another sulfide population (25%) is intimately associated with the interstitial Cpx separate from the Opx, either as swarms of droplets (1-10 μm) or as convoluted patches showing low dihedral angles and grading into vein-like extensions. The diffuse discontinous veins of coarse Cpx in the lherzolite are BMS-rich, BMS occupying the same microstructural sites as the Cpx (Fig. 4c,d). Large BMS blebs are attached to Cpx crystals that also contain concentrated sprays of hundreds of BMS inclusions orientied parallel to cleavage planes (Fig. 4d). In this peculiar sample, sulfide melt reached interconnection through the silicate matrix, as suggested by the thin sulfide veins that surround relict Opx crystals (Fig. 4c). A minor proportion of BMS (2-4%) is attached to Sp, especially S1 Sp. By contrast, no sulfide has been found in S2 symplectites.

Major element mineral compositions

Ol Mg# [= molar Mg/(Mg+Fe)] and NiO contents (Table 3) from 0.903 to 0.917 and from 0.30 to 0.43 wt%, respectively, vary little, with identical within- and inter-sample standard deviations. Sample set average is Mg# 0.9107±0.0015 and NiO 0.38±0.03 wt%. CaO contents are very low (<0.1 wt%) except in the dunite (0.22 wt%) and one harzburgite (0.24 wt% in SEY18).

Opx (Table 4) show limited within- and inter-sample compositional ranges for Mg# and CaO (0.911±0.024 and 1.91±0.34 wt%, respectively). Al_2O_3 and Cr_2O_3 are positively correlated (Fig. 5a), with the highest concentrations in the cores of the largest porphyroclasts (≥ 5 mm). However, many coarse porphyroclasts have cores depleted in Al_2O_3 and Cr_2O_3. There is no difference in concentration of Al_2O_3 and Cr_2O_3 between the smaller porphyroclasts and the grains forming intergrowths with Sp. In addition, Cr_2O_3 is low (~0.9 wt%) relative to Al_2O_3 concentrations (~3 wt%), and only a few Opx compositions plot on the extension of the abyssal Opx compositional trend, defined by the cores of similarly sized porphyroclasts (Fig. 5a; Seyler et al. 2003). This suggests that Hole 1274A Opx have been more extensively re-equilibrated to lower T than commonly observed in typical abyssal peridotites. Because Al_2O_3 and Cr_2O_3 decrease together, Cr# decreases only slightly and can thus still be used to compare the different samples.

Cpx compositions are given in Table 5. Overall, Cpx are characterized by low Al_2O_3 and Cr_2O_3 contents compared with common abyssal Cpx and both oxides decrease simultaneously (Fig. 5b). The lherzolite coarse Cpx grains are slightly zoned, with the highest

Al_2O_3, Cr_2O_3 and the lowest CaO (in integrating exsolution lamallae) contents in cores. Coarse grain rims and small Cpx grains that crystallized at the edges of coarse crystals are poorer in Al_2O_3 and Cr_2O_3 and richer in CaO. Similar compositional ranges also characterize all Cpx textural types in harzburgites, although some larger Cpx cores tend to have higher Al_2O_3 and Cr_2O_3. It is noteworthy that within a thin section, tiny Cpx in symplectites have similar compositional ranges to the cores and rims of medium-sized grains not in intimate contact with Sp. In contrast with Al_2O_3 and Cr_2O_3, Mg-numbers are systematically higher in the rims and tiny grains, indicating subsolidus Fe-Mg exchange reactions with the other silicate minerals and Sp upon cooling. Thus Al_2O_3 and Cr_2O_3 variations cannot be attributed to simple subsolidus re-equilibration and will be discussed further. TiO_2 contents are very low ≤ 0.05 wt% in most samples, increasing to 0.15 wt% in a few samples. Na_2O contents display a wide range of concentrations from near 0 up to 0.72 wt% (Fig. 2c). Most samples (75% of the sample set), including the lherzolite and the dunite, contain Cpx with very low $Na_2O \leq 0.13$ wt%; such concentrations are among the lowest Na_2O concentrations reported in abyssal peridotites. Na_2O and TiO_2 are positively correlated in these very low-Na_2O Cpx. The other samples have Cpx moderately or strongly enriched in Na_2O (0.15-0.3 wt% in six samples and >0.4 wt% in three samples, respectively) with no enrichments in TiO_2. Such high concentrations of Na_2O are at odds with the overall ultradepleted compositions of the peridotites. Cpx grains are unzoned for Na_2O and TiO_2, and, at a thin section scale, their concentration ranges are similar within grains and from grain to grain. High Na_2O samples cannot be distinguished from low Na_2O samples by any textural features or other major element compositions. Eigth of nine samples enriched in Na_2O come from the base of the hole, in the section with gabbroic intercalations and fault gouges (Fig. 2a,c). In particular, the three samples with the highest Na_2O contents (SEY23, SEY25 and HJBD13) were sampled in the bottom, close to fault gouge horizons. However, sample SEY24, extremely poor in Na_2O and TiO_2, is intercalated in the Na_2O-rich section.

Sp Cr# [= molar Cr/(Cr+Al)] vary in a very narrow range from 0.43 to 0.51 (average 0.47±0.011) in all the harzburgites and the lherzolite. Sample SEY02 is characterized by significantly lower Cr# (0.36); the dunite is only slightly higher with 0.52 (Table 6). Within-sample variations do not exceed 5%, except in one sample (SEY05) where Cr# variation is up to 10%. TiO_2 contents vary from 0.01 to 0.15 wt% (average 0.07 wt%). Such values (<0.2 wt.%) are commonly considered as a characteristic of plagioclase-free, spinel peridotites that did not react with MORB liquid at low-P (Dick 1989; Seyler and Bonatti 1997). In the entire sample set, except SEY02, Sp compositions thus define a unique, restricted, compositional field, with no correlation between Cr# and TiO_2. Average Cr# and Mg# in Sp, Ol

and Opx are well correlated from sample to sample. In Ol Mg# vs Sp Cr# diagram, Hole 1274A peridotites plot at the higher Cr# end-member (except SEY02) of the abyssal peridotite array (Fig. 6). These compositions are similar to those of dredged samples from the entire 14°-16°N region (Bonatti et al. 1992; Cannat et al. 1992, 1997) and also characterize abyssal peridotites from the 43°N area at the MAR (Shibata and Thompson 1986).

Trace elements in clinopyroxenes

Six samples have been selected for trace element study, including five harzburgites and the lherzolite SEY04. Cpx in harzburgite samples SEY03, SEY21, SEY22 and the lherzolite, have low to very low Na_2O contents ($\leq$ 0.3 wt%), whereas harzburgite samples SEY23 and SEY25 have Cpx enriched in Na_2O (0.45-0.55 wt%). Within-sample variability for REEs, Sr, Zr and Ti was investigated by analyzing Cpx of several textural occurrences (selvages on Opx, intergranular grains, core and rim, symplectites, and crack-filling); in addition, three samples were analyzed in two thin sections cut from the same slab, to study cm-scale variability. Results are presented in Table 7. Trace element concentrations show no significant intra- or inter-grain variations at a sample scale (except in sample SEY25), and as a consequence, show no texture-related variation. Thus, only average concentrations are hereafter considered for these samples. Near-homogeneous trace element contents in Cpx, suggestive of equilibrium at the thin section scale, is a typical feature of abyssal Cpx, for which with few exceptions, no significant texture-dependance is observed (Hellebrand et al. 2002). In contrast, the two grains analyzed in SEY25 show different compositions. The low-Na Cpx group has ultra-depleted trace element compositions, in accordance with the extreme depletion in major elements. HREE concentrations are two-fold lower than in Cpx from the hotspot-influenced Bouvet FZ (Johnson et al. 1990). REE absolute and relative concentrations in Site 1274 low-Na Cpx are nearly identical to Cpx from Marie Celeste FZ harzburgites in the Central Indian Ridge. The latter are also the most depleted Cpx reported for abyssal peridotites (sample ANTP84-11 in Hellebrand et al. 2002; Fig. 7). Both sets of Cpx are characterized by very steep positive Nd to Lu slope, LREE upward inflection and downward inflection in Eu. This apparent negative Eu anomaly is not coupled with a negative Sr anomaly, which would have been the signature of coexisting plagioclase (this mineral has not been observed in Hole 1274A harzburgites). In contrast, Sr is strongly enriched relative to the adjacent REEs, a feature also commonly observed in the Cpx from very depleted harzburgites, which has been explained by increased difference between Sr and REE bulk partition coefficients, as continous melting approaches the point of Cpx exhaustion (Parkinson et al. 1992). Because all these Cpx are selectively enriched

in LREEs relative to MREEs, we interpret the $(Sm/Eu)_N$ ratios >1 as an effect of Sm enrichment with respect to Eu. SEY23 REE patterns are characterized by higher concentrations in MREEs relative to HREEs and by less fractionated $(Nd/Yb)_N$ ratios. La, Ce and Sr enrichments are similar to those observed in SEY21 and SEY22 Cpx, although Na_2O is twice more concentrated. SEY25 Cpx are globally enriched in the trace elements. Starting from similar Lu and Yb concentrations, the magnitude of the enrichments increases toward the more incompatible REEs up to Ce, then slightly decreases for La. Their REE concentrations thus define patterns characterized by a concave downward shape with $(La/Ce)_N < 1$, which are unusual in abyssal peridotites but have been reported from two ultra-slow spreading ridge segments, the Gakkel peridotites in the Arctic ocean (Hellebrand et al. 2003) and the Southwest Indian Ridge near the Rodrigues Triple Junction (Toplis et al. 2003). SEY25 Cpx patterns display other unusual features for mantle peridotites equilibrated in the spinel stability field, such as strong negative Eu, Sr and Zr anomalies.

Discussion

Constraints from textures and in situ major elements

Structures, textures and compositions of the high-T mineral assemblages confirm the highly refractory compositions of Site 1274 harzburgites. No evidence for truly residual Cpx has been found. Detailed microstructures clearly demonstrate that the variability of Opx mode results from two major melt-mineral reaction events leading to different extents of replacement of the Opx either by Ol (reaction 1) or by Cpx±Sp (reaction 2), and resulting in the dm to m scale alternation of harzburgites with variable Ol/Opx and Cpx/Opx ratios observed in the drill core. In addition to modal and textural changes, melt-mineral diffusive exchange reactions occurred concurrently, which allow us to better constrain some aspects of the late magmatic history.

Interpretation of orthopyroxene resorption

A first interpretation of reaction 1 textures is to consider them as " asthenospheric " textures formed in the upwelling melting mantle (Nicolas 1986; Ceuleneer et al. 1988). In this interpretation, secondary Ol is a reaction product of Opx+Cpx+Sp incongruent melting (Kinzler and Grove 1992). On the other hand, similar textures may develop where incremental or aggregated melts, generated at deeper levels, migrate upward through residual peridotites (Daines and Kohlstedt 1993). In this second interpretation, Ol precipitation and Opx dissolution result from reaction between adiabatically ascending melts that become saturated in Ol and undersaturated in Opx and surrounding mantle (Kelemen 1990). This reaction may occur in the

convecting mantle, in regions of incipient melt focusing, where interaction between ascending partial melts and wall rock results in randomly distributed porous flow (Kelemen et al. 1995a,b; Aharonov et al. 1995), or at a higher level in the thermal boundary layer (TBL), where convection changes to, then is dominated by, conductive cooling. In Site 1274, the large (>1 mm) size of the replacive Ol grains suggests that the reaction mostly occurred at, or close to, the peridotite solidus; it continued at relatively low T and high stress as indicated by the few samples where Opx, affected by crystal plastic deformation, is also deeply corroded and replaced by tiny grains of Ol.

Reaction 2, characterized by Cpx±Sp replacing Opx, indicates that the melt was not only undersaturated in Opx (or silica) but also saturated in Cpx. Such reaction combined with reaction 1 may lead to wherlitic compositions through melt-peridotite interaction. Cpx replacing Opx textures are commonly observed in some mantle xenoliths (Zinnegrebe and Foley 1995; Klügel 2001) and lherzolite massifs (Fabriès et al. 1989) where mantle peridotites have been percolated by alkaline melts, but are not a characteristic feature of abyssal peridotites (Seyler et al. 2001). Similar textures are produced experimentally during Opx assimilation in basanitic liquid (Shaw 1999). In Shaw's (1999) experiments, crystallization of Ol and Cpx after dissolution of Opx occurs in two stages. Stage 1 produces Ol and a modified melt enriched in silica and saturated in Cpx, stage 2 crystallizes Cpx selvages on residual Opx by diffusion of Ca from the modified melt. In contrast, primitive, tholeiitic liquids, in equilibrium with mantle minerals at high pressure, become undersaturated in both Opx and Cpx and oversaturated in Ol as they begin to cool at a lower P, and Ol is the only silicate phase to crystallize within residual peridotites at the base of the TBL (Kelemen 1990; Kelemen et al. 1995a,b; Wagner and Grove 1998). Cpx precipitation will follow as Ol fractionation drives the liquids to saturation in Cpx at moderate P (0.7-1.2 GPa; Stolper 1980). At this stage, the liquid composition has significantly evolved and the peridotite has cooled well below its solidus, leading to the formation of thin metasomatic dykelets. Lack of Fe-Ti enrichments and diffuse Cpx textures in Site 1274 peridotites do not support such a conclusion. In contrast, the petrographic study indicates that both reactions, and thus the Cpx crystallization, occurred at similar conditions of low strain and high temperature of the solid matrix, prior to the formation of the lithosphere.

Additional evidence for high-T conditions comes from the observation that in spite of the fact that Opx was, in general, extensively dissolved, this mineral did no reprecipitate along with Cpx. Fractionating liquids are driven to Opx saturation if they derive from high-P partial melts that extensively reacted with wall peridotites, beyond the point of the exhaustion of Cpx (Kelemen et al. 1995a,b), or if they are silica-rich, low-P melts produced by partial melting of a

depleted peridotite, in equilibrium with a Cpx-free residue. Indeed, in many ophiolites, mantle harzburgites as refractory as Site 1274 harzburgites, which show similar textures of Opx dissolution – Ol crystallization, do contain secondary Opx (Barth et al. 2003; Dijkstra et al. 2003). In addition, these Opx have very low CaO contents (< 0.8%, Barth et al. 2003), in contrast with Site 1274 Opx (ave. CaO ~1.96%, Wo ~3.8%). Application of Brey and Kohler (1990)'s Ca-in-Opx geothermometer leads to an equilibrium temperature of ~1,250 °C at 1 GPa, suggesting that Hole 1274 peridotites cooled rapidly at depth in the TBL before uplift. This result also reflects probable dry melting Site 1274 peridotites as opposed to assumed hydrous condition in many ophiolites.

Al-Cr exchange reactions and origin of late-stage Sp and Cpx

Whereas Al_2O_3 and Cr_2O_3 behave in the opposite way during partial melting (Jacques and Green 1980), in Site 1274, both oxides decrease from core to rim in Opx, to the point where a large proportion of coarse Opx cores acquire low Al_2O_3 *and* Cr_2O_3 contents. Enhanced Al_2O_3 and Cr_2O_3 depletions indicate that re-equilibration of the Opx to lower P-T condition occurred in high-T peridotites in presence of melt, which increased Al and Cr diffusion out of Opx into the interstitial melt. This process, which occurred concurrently with the Opx resorption, lead to the complex Opx+Sp±Ol intergrowths through a suite of reactions : (i) dissolution of high-T (Al-, Cr-rich) Opx along grain boundaries and cleavages and reprecipitation of Sp, in situ, or at sites of low stress where the melt was driven by shearing of the matrix, according to the reaction $Mg(AlCr)AlSiO_6 = Mg(Al,Cr)_2O_4 + (SiO_2)_{melt}$, (ii) dissolution of adjacent Ol by modified melt locally oversaturated in silica, leading to enclosure of Ol into Sp neoblasts. During these reactions, residual Opx and Ol texturally re-equilibrated with the newly formed minerals.

Cpx selvages on Opx may result from another melt-to-mineral diffusive reaction : $0.5\ Mg_2Si_2O_6 + (CaSiO_3)_{melt} = CaMgSi_2O_6$. Minor amounts of Cpx in the Opx+Sp±Ol intergrowths, as well as the formation of the S2 symplectictes at the Opx-Ol interfaces, may also involve Cpx exsolution from Opx and/or a calcic melt component according to the reactions : $Mg_2SiO_4 + Mg(AlCr)AlSiO_6 + (CaSiO_3)_{melt} = Mg(Al,Cr)O_4 + CaMgSi_2O_6 + 0.5\ Mg_2Si_2O_6$ or $Mg_2SiO_4 + (CaAl_2SiO_6)_{melt} = CaMgSi_2O_6 + MgAl_2O_4$. In contrast, the Cpx grains that fill low-angle Ol and Ol-Opx triple junctions and the S1 symplectictes, for which no evidence for Opx- or Ol-melt reaction has been observed, probably precipitated from melt as Cpx or Cpx-Sp cotectic crystals, respectively. The ranges of Al_2O_3 and Cr_2O_3 concentrations in the Cpx likely reflect variable Al_2O_3 and Cr_2O_3 saturations of the interstitial melt under condition of rapidly decreasing

temperature as the peridotite entered into the TBL, conditions that also permit the preservation of the delicate symplectites.

Lherzolitic domains

Hole 1274A peridotites display lherzolitic domains, as exemplifyed by sample SEY04 which is enriched in both Ol and Cpx. The coarse Cpx crystals are constituants of the protogranular texture, and their orientation defines a high-T lineation; they show resorption features similar to Opx; they contain coarse (up to 4 μm) Opx exsolution lamellae; they also display Cu-rich sulfide intergrowths. All these features are in contrast with textures and compositions of late-stage Cpx (+Sp±sulfides) that overgrew the coarse Cpx as poikiloblastic rims or discrete crystals. Similar Cpx+Sp±sulfides are also abundant around reacted Opx. This second Cpx generation is characteristically small-sized, enriched in wollastonite (thin Opx exsolutions; high whole-grain CaO contents) and impoverished in Al_2O_3 and Cr_2O_3 relative to the coarse Cpx. The coarse Cpx crystals are thus interpreted to have crystallized from a sulfide-rich melt at higher P-T conditions than the late-stage Cpx grains. However, elemental compositions which are mainly controlled by melt composition (Na, Ti and incompatible trace elements) are similar between coarse and late-stage Cpx. Therefore, texture and composition relationships between the two generations of Cpx might be interpreted as the result of a dissolution – reprecipitation process at decreasing P-T conditions, that partially preserved relicts of earlier Cpx. Since late-stage Cpx in the lherzolite show mineral association, texture and compositions identical to the Cpx in the harzburgites, we suggest that Cpx saturation in the percolating melt might have been promoted by melting or selective dissolution of previous Cpx veins within residual mantle. During this process, the primary Cpx and the percolating melt evolved toward chemical equilibrium. Such melt will be especially reactive with Opx.

Constraints from trace element and mode modeling

A number of numerical models have been developed, which describe the behavior of trace elements during melt-rock interaction involving elemental exchanges both by diffusive and by mineral (e.g. with modal ± porosity changes) reactions (e.g. Godard et al. 1995; Vernières et al. 1997; Suhr et al. 1998). They show that extensive interaction between migrating melt, derived from adiabatic decompression, and depleted uppermost mantle approaches equilibrium between the melt and peridotite and rapidly depletes the melt in incompatible elements. Because the least incompatible trace elements are controlled by mineral reactions and are buffered by the peridotite, the HREE patterns in melt and solid, after melt-rock interaction,

reflect the composition of the residual solid (except at high melt/solid ratios in high-porosity channels). In contrast, concentrations of the most incompatible trace elements (LREEs) are mostly controlled by the porosity, being partially buffered by percolating melt. If melt-rock equilibration is not totally achieved, then REE patterns will show selective enrichments in LREEs quite similar to those observed in Site 1274 depleted Cpx.

As a first step in modeling the reactions, we assumed that melt-rock equilibration in Site 1274 peridotites was achieved through partial melting alone. Theoretical extents of melting of the solid residue was calculated using the concentrations of the Cpx moderately incompatible elements (Eu to Lu), that are the least sensitive to melt percolation. In this model, Cpx fractionated at the top of the melting zone from intergranular melt in equilibrium with a near-Cpx free residual harzburgite. Composition of this melt can be modeled as the composition of the last melt fraction generated at the shallowest pressure during continuous decompressional partial melting. The results of these calculations are then used as end-members to discuss the effects of additional reactions between percolating melt and residue. Our calculations, using nonmodal melting equations (Shaw 2000) and a conventional Sp-lherzolite source, cannot reproduce the M/HREE fractionations of the low-Na Cpx, whatever the melting process (batch, Raleigh, critical). To reproduce simultaneously the low Lu and Yb contents and the very low Eu/Lu ratios, melting must begin in the garnet stability field, in agreement with previous modeling of strongly depleted abyssal Cpx compositions (Johnson et al. 1990; Hellebrand et al. 2002; Brunelli et al. 2006). Polybaric, near-fractional melting models (Brunelli et al. 2006) reproduce the M-HREEs contents in our four most depleted samples after 9-10% melting in the garnet stability field, followed by 12-14% melting in the spinel stability field (Fig. 8a-c). Na-rich Cpx SEY23 cannot be reproduced in a satisfying way. Best bits are obtained after 7-9% fractional melting in the garnet stability field followed by 14-16% melting in the spinel stability field with higher residual porosity (~2-7% ; Fig. 8d). This suggests that other processes, such as melt entrapment or melt mixing, contributed to the SEY23 REE pattern. SEY25 cannot be modelled by partial melting alone, except for Lu and Yb whose concentations are nearly identical to those measured in the other samples.

Because melting reactions in the garnet stability field produced Opx (Kinzler 1997), calculated residual modes contain ~30 wt% Opx, a proportion which is very close to the Opx contents of the least reacted Site 1274 harzburgites (Opx ~28 vol%). Departure from this theoretical mode toward lower, variable, and heterogeneously distributed Opx/Ol proportions is one of the most convincing pieces of evidence for additional mineral reactions accompanying advecting melt percolation. Pervasive or poorly focused partial melt migrating upward in the

upwelling molten mantle, or in the shallow mantle at a temperature close to the peridotite solidus, enhance pyroxene dissolution and Ol crystallization, the magnitude of which increases with the amount of melt passing through the peridotite (Aharonov et al. 1995; Kelemen et al. 1995a,b; Asimow and Stolper 1999). Thus, an alternative model would be to assume that the peridotite underwent a lower degree of adiabatic melting than the one calculated above, leaving a substantial amount of residual Cpx (for instance ~10% upon 12% melting in the spinel field) that would disappear by additional dissolution. In this case, residual intergranular melt would equilibrate with Cpx-free harzburgites characterized by low and highly fractionated REE contents. During this process, both Opx and Cpx are subject to dissolution with Opx more rapidly dissolving as pressure decreases (Kelemen et al. 1995b). However, Site 1274 Opx-rich harzburgites are also devoid of residual Cpx, it is thus likely that low-P melt-rock interaction involved a harzburgite mantle already depleted in Cpx and, thus, that partial melting did start in the garnet stability field.

Selective LREE enrichments in the depleted Cpx, and the occurrence of Na-rich, REE-enriched Cpx (samples SEY23 and 25), may reflect incomplete or local equilibrium between percolating melt and residue, the former being more enriched in REE than the latter, or may be explained by a later event that occurred during or just after the Cpx crystallization (Navon and Stolper 1987; Bodinier et al. 1990; Takazawa et al. 1992), in relation to the presence of former melt channels.

Additional constraints from BMS distribution

BMS provide further evidence supporting variable degrees of reactions of a highly refractory mantle with a percolative melt. It is now well demonstrated that S behaves as a moderately incompatible element during mantle melting, because basaltic melts dissolve five to ten times more S than the estimated S content of the upper mantle (Lorand 1991; and ref. therein). At 1.5 GPa, conventional fractional melting predicts total consumption of BMS for $F \leq 12\text{-}16$ % if the depleted MORB mantle contains about 150 ppm S (Saal et al. 2002 ; Luguet et al. 2003). Because the solubility of S decreases with increasing pressure (Mavrogènes and O'Neill, 1999), a partial melting event starting in the garnet lherzolite stability field would allow BMS to persist in residual solids at higher F (≤20%). The near-zero S contents of certain Site 1274 Opx-rich harzburgites are therefore consistent with a high degree of partial melting that has progressed beyond complete resorption of the sulfides.

The remainder of Site 1274 harzburgites are much too rich in BMS to be interpreted as simple melting residues. Assuming that all of the S is residing in BMS, the highest BMS

content (0.1 vol%) corresponds to c.a. 300±30 ppm S (based on pentlandite and chalcopyrite S concentrations of 33 and 35 wt%, respectively; unpublished data). This bulk-rock S content is twice the " best estimate " for the convecting depleted mantle. In theory, the conventional fractional melting model predicts a regular decrease of S contents negatively correlated with melt depletion indexes such as Ol Mg# and Sp Cr#. There is no such correlation in Site 1274 harzburgites which, on the contrary, display huge variations of BMS modal abundances, sometimes at the hand-sample scale, in spite of nearly constant Ol Mg# and Sp Cr#. Such heterogeneous distribution can be understood if BMS are " cumulate minerals " of a heterogeneously distributed percolating melt in disequilibrium with harzburgites. The common occurrence of BMS in microstructural sites of melt-rock reactions (Opx-Ol and Cpx-Opx) provide strong support to this interpretation, as does the overabundance of Cu-rich sulfides in Opx-hosted inclusions and of native copper in intergranular BMS that have experienced strong reduction by serpentinization fluids. The assemblage Pn+Cp+Bo (which was protected from serpentinization) is characteristic of oceanic peridotites that have been refertilized in Cpx+Sp by basaltic melts (Lorand 1988; Luguet et al. 2003). Experimental phase diagrams in the Cu-Fe-Ni-S system (Craig and Kullerud 1969) show this assemblage to be a crystallization product of a Cu-enriched Ni-Fe sulfide melt with metal/sulfur atomic ratio >1.

The fact that the highest BMS concentrations correspond to rocks with high (> 0.1) Cpx/Opx modal ratios (SEY03, SEY04, SEY23) outlines the main effect of Cpx fractionation. As suggested above, Cpx crystallization in Site 1274 harzburgites was promoted by rapid temperature decrease at relatively high pressure (~0.8-1 GPa). Such P-T conditions enhance BMS precipitation by reducing the solubility of S in the percolating melt (Naldrett 1989). In the lherzolite SEY04, the volume of sulfide liquid was high enough for sulfide melt films to be locally interconnected through the interstitial pores of the silicate matrix (Fig. 4c). Experimental data (Gaetani and Grove 1999) suggests that interconnection can occur for 0.1 vol% intergranular sulfides, which is very close to the BMS modal abundance measured in this sample. It is likely that, after such a massive coprecipitation of BMS and Cpx, S was exhausted from the residual silicate melt and no BMS precipitated inside S2 symplectites.

The BMS embedded in Opx porphyroclasts is a common occurrence in ophiolitic and abyssal harzburgites and interpreted as incompletely extracted residual sulfides that have survived partial melting (Lorand 1988; Luguet et al. 2003). This interpretation does not pertain to Site 1274 harzburgites that experienced high degrees of melting beyond complete resorption of BMS. In these rocks, the BMS embedded in Opx contain a high proportion of Cu-rich minerals and are often rimmed by Sp or discrete Cpx crystals. These chemical and

microstructural criteria suggest that BMS actually precipitated from trapped, Cu-rich, melts and then infiltrated the corroded Opx at temperatures below the peridotite solidus via the numerous corrosion embayments and fractures. Cu-Ni sulfide melts have depressed solidus temperatures compared to major silicates of anhydrous peridotites (<1,000 °C vs. 1,300 °C at 1 GPa) and high wetting capacity (Ballhaus et al 2001), which can explain the secondary sulfide inclusion networks within the Opx.

A two-stage partial melting/melt-rock reaction model for Site 1274 peridotites ?

The wealth of textural, mineralogical and geochemical data obtained from this study yields some contradictions and inconsistencies. A high degree of melting of peridotite, starting in the garnet stability field, is inconsistent with normal mantle temperature inferred from the chemistry of the basalts and gabbros sampled north of the 15°20'N FZ, which have normal MORB compositions (Dosso et al. 1991, 1993; Kelemen 2003) and from the structure of the lithosphere, which is typical of a slow-spreading ridge (thin crust but thick lithospheric mantle, in which a large amount of gabbroic rocks have frozen; Cannat 1996). The Cu-Ni-rich composition of the metasomatic BMS also argues against a refractory percolating melt.

We propose to solve these inconsistencies by assuming that the convective mantle at the Mid-Atlantic Ridge, 15°-16°N, contained harzburgitic blobs that have already been affected by early high-P history of melt depletion and refertilization before upwelling and remelting beneath the present-day ridge. Such a two-stage petrogenetic model has been suggested for other abyssal peridotites from ultra-slow spreading ridges (Seyler et al. 2004) and is supported by Os model ages indicating a long term Re depletion (Brandon et al. 2000; Alard et al. 2005). For this to apply for Hole 1274A peridotites requires the garnet signature and the high Opx contents of the least reacted harzburgites.

Pyroxene layering in the peridotites may be partially inherited from former pyroxenite veins. This pyroxenitic component preferentially melted to produce a melt undersaturated in Opx and saturated in Cpx. Experimental melting of Cpx-rich lithologies with MORB affinity demonstrate that melts have major element compositions in the range of normal MORB compositions (Pickering-Witter and Johnston 2000; Schwab and Johnston 2001). In addition, experimental melting of Cpx+Sp layer enclosed within a peridotite matrix, with bulk composition similar to MORB composition, releases a melt strongly undersaturated in Opx, which upon reaction with surrounding residual harzburgite, yields normal MORB liquid and residual Ol+Sp assemblage (Bulatov et al. 2002). Mantle pyroxenites are four to five times more enriched in S and Cu than fertile lherzolite (Lorand 1991). Therefore a high degree of

melting of Cpx-rich veins may produce a melt saturated in Cu-rich sulfide phases. This melt is just as capable to precipitate Cu-rich BMS as is a low-degree melt of peridotite of similar major element composition in the percolated mantle column. In this interpretation, the coarse Cpx+Ol+sulfides assemblages in the lherzolite sample represent relics of early cumulate veins that partially melted and/or reacted with peridotitic melt. Lack of a geochemical anomaly in the regional basalts does not preclude our model, as very small amounts of Cpx-rich melt will be highly diluted after mixing with partial melts from the melting of surrounding depleted peridotites that had some remaining Cpx.

Concluding remarks

Leg 209 Hole 1274A harzburgites differ from common abyssal peridotites by extreme refractory compositions and by well-developed textures of Opx dissolution and Ol+Cpx+Sp+sulfides crystallization. They also show more extensive melt-mineral elemental exchange reactions, resulting in lower Al and Cr contents in residual Opx and in anomalously depleted, U-shaped REE patterns in Cpx. Although Site 1274 peridotites may resemble some ophiolitic and forearc mantle harzburgites, lack of secondary Opx and higher temperature of equilibration show that the extra-depletion was not caused by late-stage hydrous melting. Characteristics of Site 1274 samples indicate reaction with a melt in strong disequilibrium with the peridotite matrix at a temperature close to its solidus.

Acknowledgements This research used samples and data supplied by the Ocean Drilling Program (ODP). ODP is sponsored by the U.S. National Science Foundation (NSF) and participating countries under management of Joint Oceanographic Institutions (JOI), Inc. We thank D. Brunelli for discussion, and B. Boyer for his assistance with the SIMS analyses. Comments from two anonymous reviewers are gratefully acknowledged. Funding for this research was provided by Centre National de la Recherche Scientifique-Institut National des Sciences de l'Univers (Programme Dynamique et Evolution de la Terre Interne).

References

Alard O, Luguet A, Pearson N J, Griffin W L, Lorand, J-P, Gannoun A, Burton KW, O'Reilly SY (2005) In-situ Os analyses bridging the isotopic gap between abyssal peridotites and Mid-Oceanic Ridge Basalts. Nature 436: 1005-1008

Aharonov E, Whitehead JA, Kelemen PB, Spiegelman M (1995) Channeling instability of upwelling melt in the mantle. J Geophys Res 100: 20433-20450

Anders E., Grevesse N (1989) Abundances of the elements: Meteoritic and solar. Geochim Cosmochim Acta 53: 197–214

Asimow PD (1999) A model that reconciles major- and trace-element data from abyssal peridotites. Earth Planet Sci Lett 169: 303-319

Asimow PD, Stolper EM (1999) Steady-state mantle-melt interactions in one dimension : I. Equilibrium Transport and melt focusing. J Petrol 40: 475-494

Ballhaus C, Tredoux M, Spaeth A. (2001) Phase relations in the Fe-Ni-Cu-PGE-S system at magmatic temperature and application to massive sulfide ores of Sudbury Igneous Complex. J Petrol 42: 1991-1926

Barth MG, Mason PRD, Davies GR, Dijkstra AH, Drury MR (2003) Geochemistry of the Othris Ophiolite, Greece: Evidence for refertilisation? J Petrol 44 : 1759-1785

Bodinier JL, Vasseur G, Dupuy C, Fabriès J (1990) Mechanisms of mantle metasomatism : Geochemical evidence from the Lherz orogenic peridotite. J Petrol 31: 597-628

Bonatti E, Peyve A, Kepezhinskas P, Kurentsova N, Seyler M, Skolotnev S, Udintsev G (1992) Upper mantle heterogeneity below the Mid-Atlantic Ridge, 0–15°N. J Geophys Res 97: 4461–4476

Bottazzi P, Ottolini L, Vannucci R, Zanetti A (1994) An accurate procedure for the quantification of rare elements in silicates. Proc Ninth Intern Conf on Secondary Ion Mass Spectrometry SIMS IX. John Wiley & Sons New York, pp 927-930

Brandon, AD, Snow JE, Walker RJ, Morgan JW, Mock TD (2000) $^{190}Pt/^{186}Os$ and $^{187}Re/^{187}Os$ systematics of abyssal peridotites. Earth Planet Sci Lett 177: 319–335

Brey GP, Kohler T (1990) Geothermobarometry in 4-phase lherzolites. 2. New thermobarometers and practical assessment of existing thermobarometers. J Petrol 31: 1353-1378

Brunelli D, Seyler M, Cipriani A, Ottolini L, Bonatti E (2006) Discontinuous Melt Extraction and Weak Refertilization of Mantle Peridotites at theVema Lithospheric Section (Mid-Atlantic Ridge). J Petrol 47: 745-771

Bulatov VK, Girnis AV, Brey GP (2002) Experimental melting of a modally heterogeneous mantle. Mineral Petrol 75: 131-152

Cannat M (1996) How thick is the magmatic crust at slow-spreading oceanic ridges ?. J Geophys Res 101: 2847-2857

Cannat M, Bideau D, Bougault H (1992) Serpentinized peridotites and gabbros in the Mid-Atlantic Ridge axial valley at 15°37'N and 16°52'N. Earth Planet Sci Lett 109: 87–106

Cannat M, Lagabrielle Y, de Coutures N, Bougault H, Dmitriev L, Fouquet Y (1997) Ultramafic and gabbroic exposures at the Mid-Atlantic Ridge: Geological mapping in the 15°N region. Tectonophysics 279: 193-213

Ceuleneer G, Nicolas A, Boudier F (1988) Mantle flow patterns at an oceanicspreading centre: the Oman peridotite record. Tectonophysics 151: 1-26

Craig JR, Kullerud G (1969) Phase relations in the Cu-Fe-Ni-S system and their applications to magmatic ore deposits. In: Magmatic Ore Deposits, Econ Geol Monog 4, pp 343-358

Daines MJ, Kohlstedt DL (1993) Melting and melt movement in the Earth. Phys Sci and Engineering 342: 43-52

Dick HJB (1989) Abyssal peridotites, very slow spreading ridges and ocean ridge magmatism. In: Saunders AE, Norris MJ (eds) Magmatism in the Ocean Basins. Geolog Soc Spec Public 42, pp 71-105

Dijkstra AH, Barth MG, Drury MR, Mason PRD, Vissers RLM (2003) Diffuse porous melt flow and melt-rock reaction in the mantle lithosphere at a slow-spreading ridge: A structural petrology and LA-ICP-MS study of the Othris Peridotite Massif (Greece). Geochem Geophys Geosyst DOI: 10.1029/2001GC000278.

Dosso L, Bougault H, Schilling JG, Joron JL (1991) Sr-Nd-Pb geochemical morphology between 10° and 17°N on the Mid-Atlantic Ridge: a new MORB isotope signature. Earth Planet Sci Lett 106: 29-43

Dosso L, Bougault H, Joron JL (1993) Geochemical morphology of the north Mid-Atlantic Ridge, 10°-24° N, trace element-isotope complementarity. Earth Planet Sci Lett 120: 443-462

Elthon D (1992) Chemical trends in abyssal peridotites: Refertilization of depleted suboceanic mantle. J Geophys Res 97: 9015–9025

Escartin J, Cannat M (1999) Ultramafic exposures and the gravity signature of the lithosphere near the Fifteen-Twenty Fracture Zone (Mid-Atlantic Ridge, 14°-16.5°N). Earth Planet Sci Lett 171: 411-424

Fabriès J, Bodinier JL, Dupuy C, Lorand JP, Benkerrou C (1989) Evidence of modal metasomatism in the orogenic spinel lherzolite body from Caussou (Northern Pyrenees, France). J Petol 30: 199-228

Fujiwara T, Lin J, Matsumoto T, Kelemen PB, Tucholke BE, Casey J (2003) Crustal evolution of the Mid-Atlantic Ridge near the Fifteen-Twenty Fracture Zone in the last 5 Ma. Geochem. Geophys. Geosyst DOI: 10.1029/2002GC000364.

Gaetani GA, Grove TL (1999) Wetting of mantle olivine by sulphide melt: implications for Re/Os ratios in the mantle peridotite and late-stage core formation. Earth Planet Sci Lett 169: 147-163

Godard M, Bodinier JL, Vasseur G (1995) Effects of mineralogical reactions on trace element redistributions in mantle rocks during percolation processes: A chromatographic approach. Contrib Mineral Petrol 133: 449-461

Godard M, Seyler M, Harvey J, Alard O (2004) Geochemical Study of Mid Atlantic Ridge Peridotites from 15°N: Preliminary Results from ODP Site 1272 and ODP Site 1274. EOS Trans AGU 85 (47) Fall Meet Suppl Abst V22A-05

Hellebrand E., Snow JE, Hoppe P, Hofman AW (2002) Garnet-field melting and late-stage refertilization in 'residual' abyssal peridotites from the Central Indian Ridge. J Petrol 43: 2305-2338

Hellebrand E, Snow JE (2003) Deep melting and sodic metasomatism underneath the highly oblique-spreading Lena Trough (Arctic Ocean). Earth Planet Sci Lett 216: 283-299

Jacques AL, Green DH (1980) Anhydrous melting of peridotite at 0-15 kb pressure and the genesis of tholeiitic basalts. Contrib Mineral Petrol 73: 287-310

Johnson KTM, Dick HJB, Shimizu N (1990) Melting in the oceanic upper mantle: an ion microprobe study of diopsides in abyssal peridotites. J Geophys Res 95: 2661-2678

Johnson KTM, Dick HJB (1992) Open system melting and the temporal and spatial variation of peridotite and basalt compositions at the Atlantis II F.Z. J Geophys Res 97: 9219-9241

Kelemen PB (1990) Reaction between ultramafic rock and fractionating basaltic magma, I. Phase relations, the origin of calc-alkaline magma series, and the formation of discordant dunite. J Petrol 31: 51-98

Kelemen PB, Hirth G, Shimizu N, Spielgelman M, Dick HJB (1997) A review of melt migration processes in the adiabatically upwelling mantle beneath oceanic spreading ridges. Philantropic Transactions Royal society of London 355: 283-318

Kelemen PB, Shimizu N, Salters VJM (1995a) Extraction of mid-ocean-ridge basalt from the upwelling mantle by focused flow of melt in dunite channels. Nature 375: 747-753

Kelemen PB, Whitehead JA, Aharonov E, Jordahl KA (1995b) Experimentson flow focusing in soluble porous media, with applications to melt extractionfrom the mantle. J Geophys Res 100: 475-496

Kelemen, P.B., Kikawa, E., Miller, D.J., et al. (2004) Proc ODP Init Repts 209 [CD-ROM]. Available from: Ocean Drilling Program, Texas A&M University, College Station TX 77845-9547, USA. Proc ODP Init Repts 209 [Online]. Available from World Wide Web: http://www-odp.tamu.edu/publications/209_IR/209ir.htm

Kelemen PB (2003) Igneous crystallization beginning at 20 km beneath the Mid-Atlantic Ridge, 14° to 16° N. EOS Trans AGU 84 (46) Fall Meet Suppl Abst V22H-03 invited

Kinzler RJ (1997) Melting of mantle peridotite at pressures approaching the spinel to garnet transition: application to mid-ocean ridge basalt petrogenesis. J Geophys Res 102: 853-874

Kinzler RJ, Grove TL (1992) Primary magmas of mid-ocean ridge basalts, 2. Applications, J Geophys Res 97: 6907-6926

Klügel A (2001) Prolonged reactions between harzburgite xenoliths and silica-undersaturated melt: implications for dissolution and Fe-Mg interdiffusion rates of orthopyroxene. Contrib Mineral Petrol 141: 1-14

Lorand J-P (1988) The Cu-Fe-Ni sulfide assemblages of tectonic peridotites from the Maqsad district, Sumail ophiolite, Southern Oman: implications for the origin of the sulfide component in the oceanic upper-mantle. In "The ophiolites of Oman", F. Boudier et A. Nicolas, (eds). Tectonophysics 151: 57-74

Lorand J-P. (1991) Sulfide petrology and sulfur geochemistry of orogenic lherzolites : a comparative study between Pyrenean bodies (France) and the Lanzo massif (Italy). In: Menzies MA et al. (eds) Orogenic Lherzolites and Mantle Processes. J Petrol, pp 77- 95

Lorand, J-P, Grégoire M (2006) Petrogenesis of base metal sulfides of some peridotites of the Kaapvaal craton (south Africa). Contrib Mineral Petrol 151: 495-520

Luguet A, Lorand J-P, Seyler M (2003) A coupled study of sulfide petrology and highly siderophile element geochemistry in abyssal peridotites from the Kane Fracture Zone (MARK area, Mid-Atlantic Ridge). Geochim Cosmochim Acta 67: 1553-1570

Mavrogènes JA, O'Neill HSC (1999) The relative effects of pressure, temperature and oxygen fugacity on the solubility of sulfide in mafic magmas. Geochim Cosmochim Acta 63: 1173–1180.

Naldrett AJ (1989) Sulfide melt crystallization temperatures, solubilities in silicate melts, and Fe, Ni, and Cu partitioning between basaltic magmas and olivine. In: Whitney JA, and Naldrett AJ, (eds) Ore depositions associated with magmas. Reviews in Econ Geol 4: 5-20

Navon O, Stolper E (1987) Geochemical consequences of melt percolation: the upper mantle as a chromatographic column. J Geol 95: 285-307

Nicolas A (1986) A melt extraction model based on structural studies in mantle peridotites. J Petrol 27: 999-1022

Parkinson IJ, Pearce JA, Thirlwall MF, Johnson KTM, Ingram G (1992) Trace element geochemistry of peridotites from the Izu-Bonin-Mariana forearc, Leg 125. In: Fryer P, Pearce JA, Stokking LB et al. (eds) Proc ODP Sci Results 125. Ocean Drilling Program, College Station, Texas, pp 487-506.

Pickering-Witter J, Johnston AD (2000) The effects of variable bulk composition on the melting systematics of fertile peridotitic assemblages. Contrib Mineral Petrol 140: 190-211

Ross K, Elthon D (1997) Extreme incompatible trace-element depletion of diopside in residual mantle from south of the Kane Fracture Zone. In: Karson JA, Cannat M, Miller DJ, Elton D (eds.) Proc ODP Sci Results, vol 153. College Station, Texas, pp 277-284

Saal A.E., Hauri E.H., Langmuir C.H., Perfit M.R. (2002) Vapour undersaturation in primitive mid-ocean-ridge basalt and the volatile content of Earth's upper mantle. Nature 419: 451-455

Schwab BE, Johnston AD (2001) Melting systematics of modally variable, compositionally intermediate peridotites and the effects of mineral fertility. J Petrol 42: 1789-1811

Seyler M, Bonatti E (1997) Regional-scale melt-rock interaction in lherzolitic mantle in the Romanche Fracture Zone (Atlantic ocean). Earth Planet Sci Lett 146: 273-287

Seyler M, Cannat M, Mével C (2003) Evidence for major-element heterogeneity in the mantle source of abyssal peridotites from the Southwest Indian Ridge (52° to 68°E). Geochem Geophys Geosyst DOI: 10.1029/2002GC000305

Seyler M, Lorand JP, Toplis M, Godard G **(**2004**)** Asthenospheric metasomatism beneath the mid-oceanic ridge: Evidence from depleted abyssal peridotite. Geology 32: 301-304

Seyler M, Toplis MJ, Lorand JP, Luguet A, Cannat M (2001) Clinopyroxene microtextures reveal incompletly extracted melts in abyssal peridotites. Geology 29: 155-158

Shaw CSJ (1999) Dissolution of orthopyroxene in basanitic magma between 0.4 and 2 GPa: further implications for the origins of Si-rich alkaline glass inclusions in mantle xenoliths. Contrib Mineral Petrol 135: 114-132

Shaw DM (2000) Continuous (dynamic) melting theory revisited. The Canadian Mineralogist 38: 1041-1063

Shibata T, Thompson G (1986) Peridotites from the Mid-Atlantic Ridge at 43° N and their petrogenetic relation to abyssal tholeiites. Contrib Mineral Petrol 93: 144-159

Stolper E (1980) A phase diagram for mid-ocean ridge basalts: Preliminary results and implications for petrogenesis. Contrib Mineral Petrol 74: 13–27

Streckeisen A (1976) To each plutonic rock its proper name. Earth Sci Rev 12 : 1-33

Suhr G, Seck HA, Shimizu N, Günther D, Jenner G (1998) Infiltration of refractory melts into the lowermost oceanic crust: evidence from dunite- and gabbro-hosted clinopyroxenes in the Bay of Islands Ophiolite. Contrib Mineral Petrol 131: 136-154

Takazawa E, Frey FA, Shimizu N, Obata M, Bodinier JL (1992) Geochemical evidence for melt migration and reaction in the upper mantle. Nature 359: 55-58

Toplis MJ, Seyler M, Mével C (2003) Trace element concentrations of clinopyroxenes in peridotites from the eastern section of the ultra-slow spreading Southwest Indian ridge (40°E-69°E). EGS Geophys Res Abstracts vol 5: 07305

Vernières J, Godard M, Bodinier JL (1997) A plate model for the simulation of trace elements during partial melting and magma transport in the Earth's upper mantle. J Geophys Res 102: 24771-24784

Wagner TP, Grove TL (1998) Melt/harzburgite reaction in the petrogenesis of tholeiitic magma from Kilauea volcano, Hawaii. Contrib Mineral Petrol 131: 1-12

Zinnegrebe E, Foley SF (1995) Metasomatism in mantle xenoliths from Gees, West Eiffel, Germany: evidence for the genesis of calk-alcaline glasses and metasomatic Ca-enrichment. Contrib Mineral Petrol 122: 75-96

Figure captions

Fig. 1 Location and lithologies of ODP Leg 209 drill sites, shown on bathymetric map from Fujiwara et al. (2003).

Fig. 2 ODP Leg 209 Hole 1274A. (a) Stratigraphic summary of lithologies with a graphical depiction of the recovery for each interval (TD = total depth; after Kelemen et al. 2004). (b) Distribution of magmatic sulfides in twenty-five samples. (c) Ranges of Na_2O contents in clinopyroxenes from thirty-six samples.

Fig. 3 Photomicrographs of Site 1274 harzburgite textures, indicative of reactions with a porous melt. (a) Wedge-shaped fracture in a coarse orthopyroxene porphyroclast. The broken part had slightly rotated and fracture is filled by secondary clinopyroxene. In bottom, large embayment filled with a single olivine grain. Crossed polarizers. (b) Detail of oval, resorbed orthopyroxene. Left end of the crystal was corroded by melt that penetrated following a cleavage plane. Secondary olivine (ol) and clinopyroxene (cpx; colored in white for clarity) now fill the space. Transmitted light. (c) Right end of same orthopyroxene porphyroclast (opx1) as in (b) formerly percolated by melt that followed the cleavages before precipitating spinel (sp; dark brown) and clinopyroxene (cpx; colored in white) intergrowth. This new material seals texturally re-equilibrated subgrains of the orthopyroxene (opx2), and continues as intergranular extensions between adjacent olivine (arrows). Transmitted light. (d) Back scattered electron image of clinopyroxene (light gray) and spinel (white) S1 symplectite, filling serpentinized olivine (ol; dark) triple junction. (e) Back scattered electron image of clinopyroxene (light gray), orthopyroxene (gray) and spinel (white) S2 symplectite developed at the interface of orthopyroxene porphyroclast (opx1) and olivine (ol). Scale bar for all micrographs represents 500 μm.

Fig. 4 (a-d) Photomicrographs of Site 1274 lherzolite sample SEY04. (a) Part of vein-like, coarse-grained clinopyroxene in serpentinized olivine matrix. Arrow 1 shows embayment filled with secondary olivine. Arrow 2 shows intergranular extension of the grain boundary in adjacent (now serpentinized) olivine matrix. Arrows 3 show a stringer of Al-Cr-poor clinopyroxene rimming the coarse clinopyroxene. Transmitted light. (b) Coarse clinopyroxene (cpx) developed at the border of altered orthopyroxene porphyroclast (opx), and replacing it

deeply inside. Note that the two pyroxenes share common (001) planes. Arrows at the top show a rim of secondary Al-Cr-poor clinopyroxene (left) grading to clinopyroxene-spinel intergrowth (right). The latter surrounds almost completely the orthopyroxene. Transmitted light. (c) Rims of coarse clinopyroxene with large BMS blebs attached (arrow 1). These rims extent in thin intergranular veins associated with spinel (sp) and sulfide (arrows 2), suggesting that the melt reached interconnection through the silicate matrix. Reflected light. (d) BMS grains enclosed in cleavage planes of a coarse clinopyroxene (white and arrows 1). Note the large BMS grain attached on the clinopyroxene (arrow 2). Reflected light. (e) Continuous poikiloblastic clinopyroxene rim sealing BMS micrograins (white and arrow) at the outer margin of a highly resorbed orthopyroxene. Reflected light. (f) A large BMS grain penetrating into a corroded orthopyroxene (arrow 1). Note the secondary sulfide inclusion networks inside the orthopyroxene (arrow 2). Scale bar for all micrographs represents 500 μm.

Fig. 5 Cr_2O_3 vs Al_2O_3 (wt%) in pyroxenes of Hole 1274A peridotites. Point symbols represent sample averages. (a) Pc = porphyroclast cores; Sym = in S2 symplectites and other intergrowths with spinel. Field of abyssal peridotite orthopyroxene porphyroclast cores ≥ 5mm (Seyler et al. 2003). (b) Pc = coarse grain cores; Gc = medium grain cores; Pr/Gr = coarse and medium grain rims; IG = small interstitial grains and selvages on orthopyroxene; Sym = in S1 and S2 symplectites and in intergrowths with orthopyroxene and spinel. Field of abyssal peridotite residual clinopyroxene cores (Seyler et al. 2003).

Fig. 6 Olivine forsterite contents vs spinel Cr# [= molar Cr / (Cr+Al)] in Hole 1274A peridotites. Point symbols represent sample averages. Bars represent 1σ sample variations. Field of Mid-Atlantic Ridge (MAR) peridotites from Seyler et al. (2003). Field of peridotites from 43°N at the MAR after Shibata and Thompson (1986).

Fig. 7 Chondrite-normalized clinopyroxene rare earth element, Sr, Zr and Ti patterns of Hole 1274A peridotites. (a) Low-Na clinopyroxenes. (b) High-Na clinopyroxenes. Upper hatched field represents the range for abyssal peridotites after Johnson et al. (1990), Ross and Elthon (1997), Hellebrand et al. (2002) and Brunelli et al. (2006). Lower hatched field is the range for Marie Celeste Fracture Zone peridotites in the Central Indian Ocean after Hellebrand et al. (2002). CI chondrite normalization values from Anders and Grevesse (1989).

Fig. 8 Results of polybaric continuous (critical) melting models in the garnet, then the spinel peridotite fields (thick dashed lines). Equations for continuous melting from Shaw (2000). Polybaric model and melting parameters (initial and melt modes, source composition, melt/peridotite partition coefficients) same as in Brunelli et al. (2006). Departure of Site 1274 samples from calculated patterns for Sm to La is attributed to late-stage chromatographic fractionation (not modeled here).

colour figure

Click here to download high resolution image

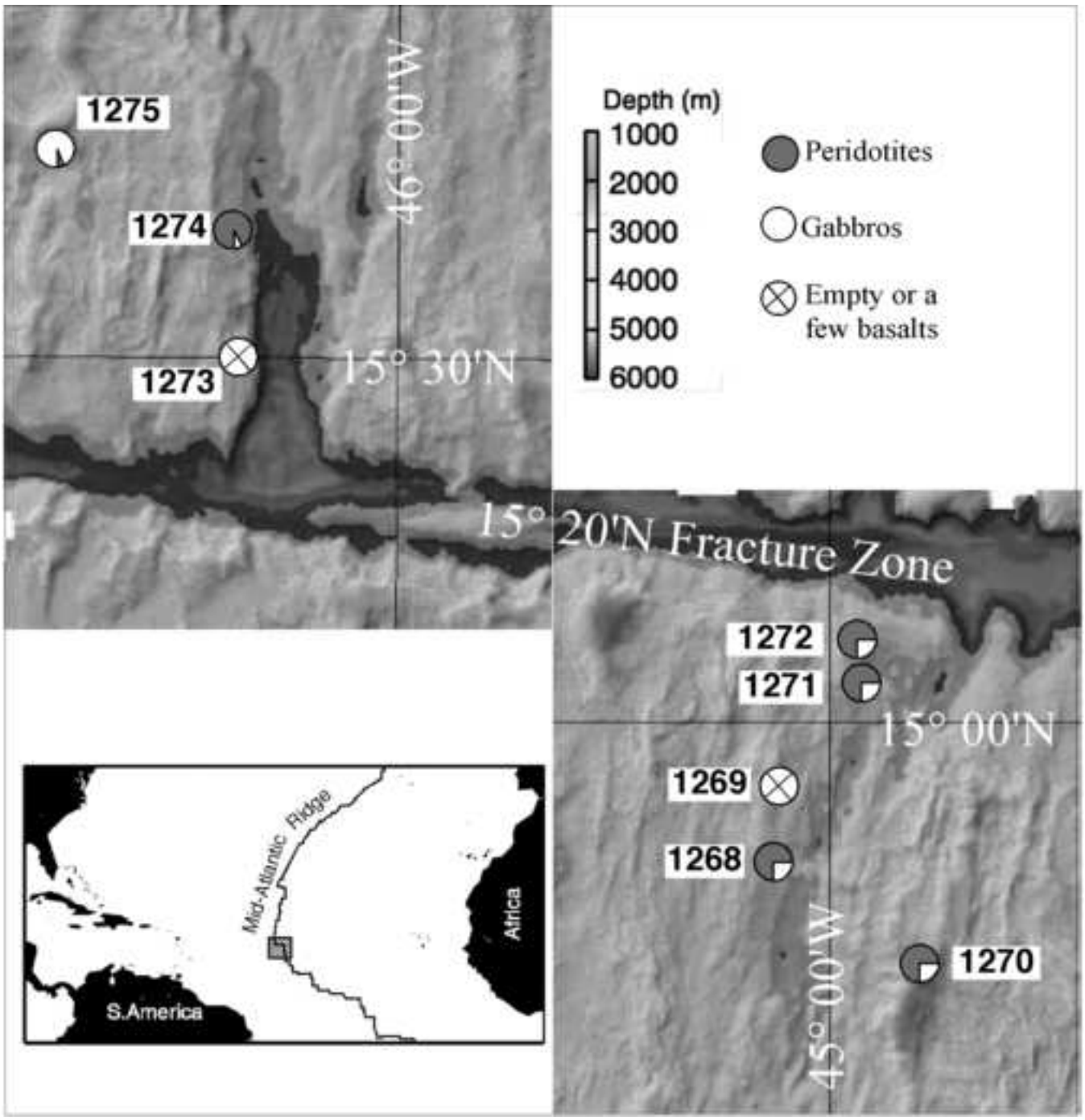

line figure

Click here to download line figure: fig02.eps

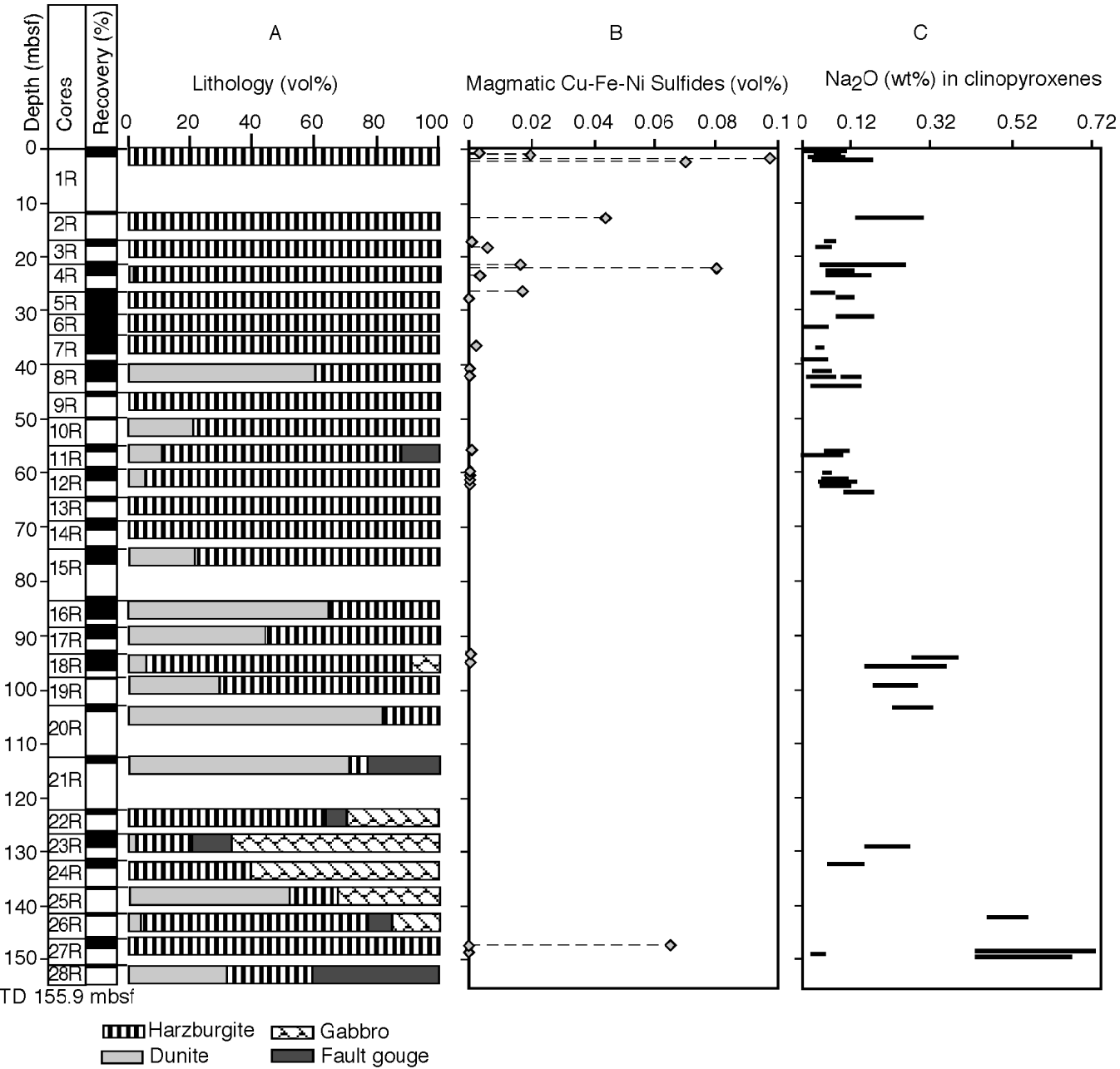

colour figure

Click here to download high resolution image

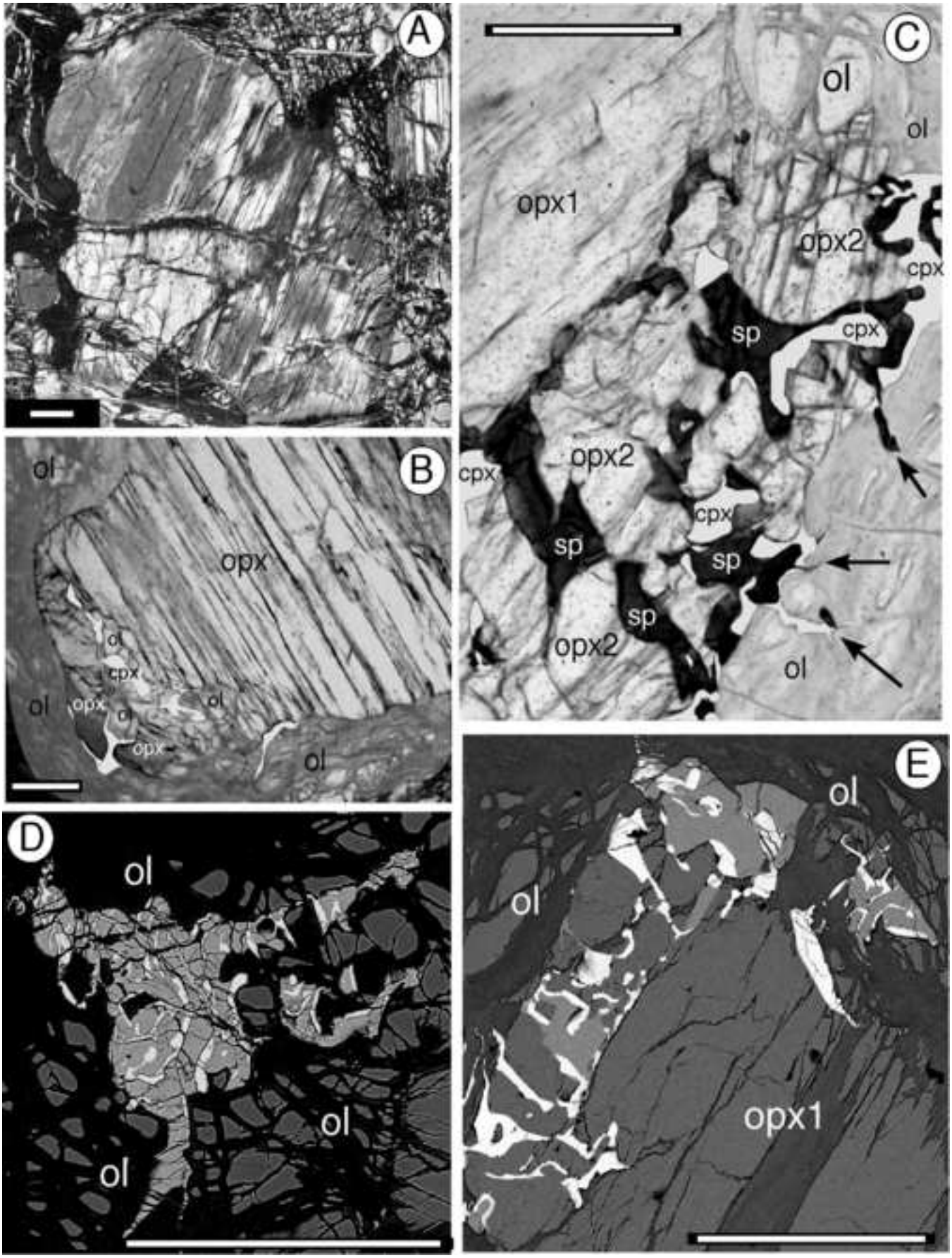

colour figure

Click here to download high resolution image

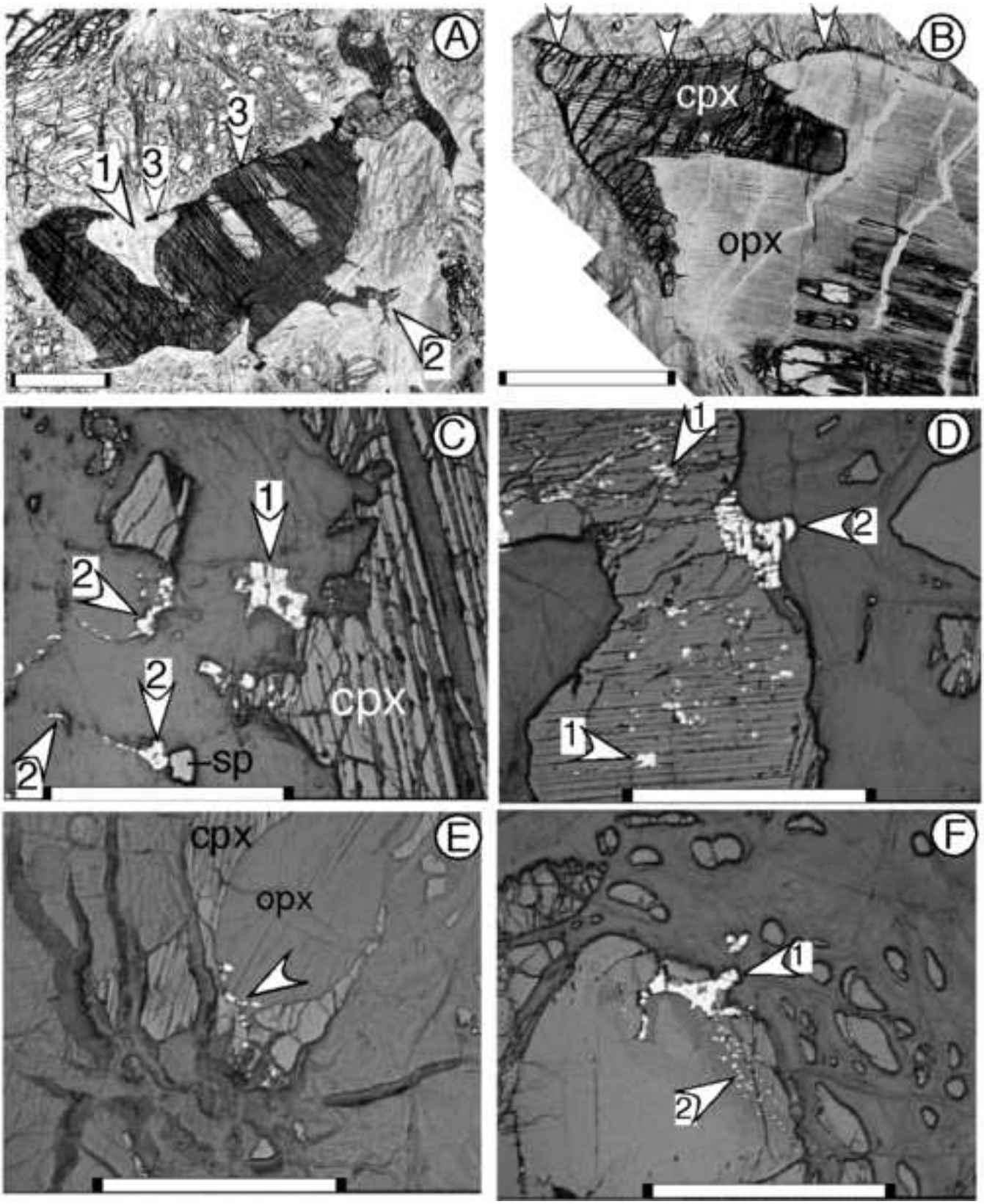

line figure

Click here to download line figure: fig05.eps

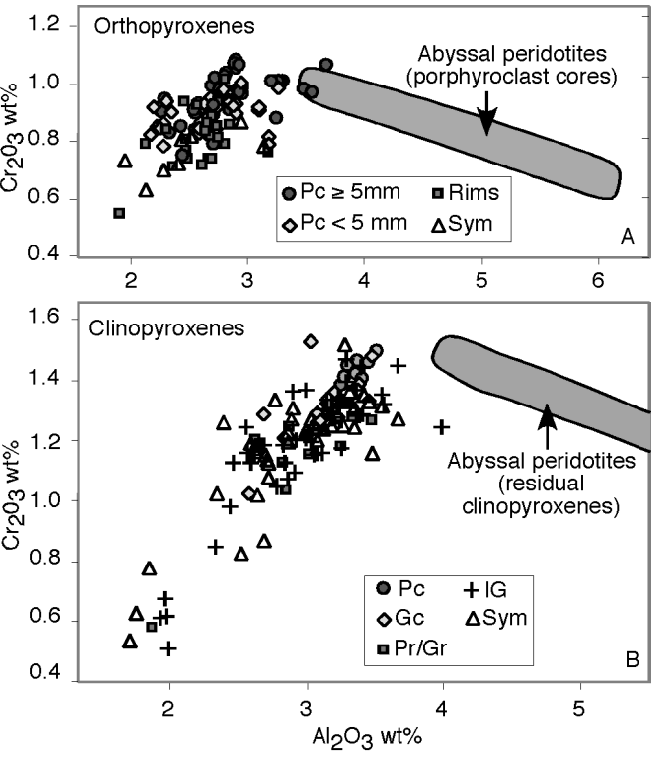

line figure

Click here to download line figure: fig06.eps

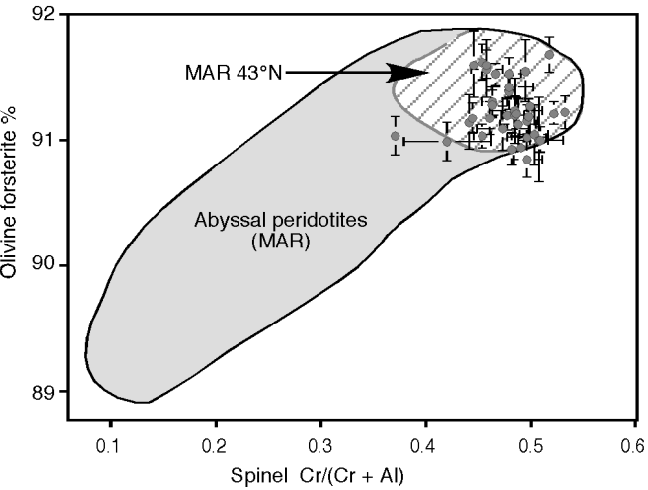

line figure

Click here to download line figure: fig07.eps

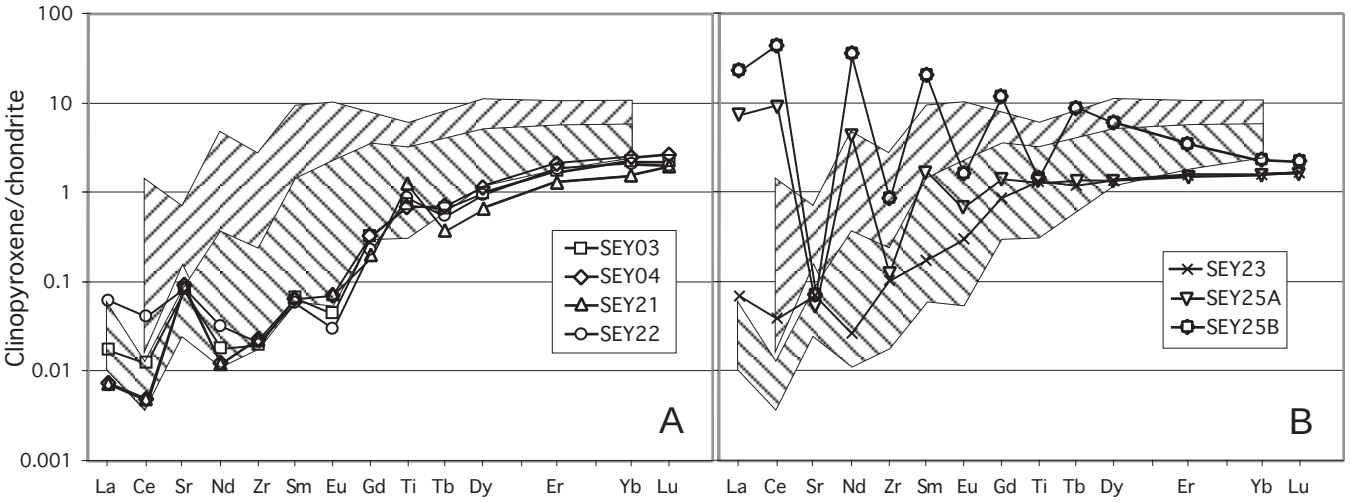

line figure

Click here to download line figure: fig08.eps

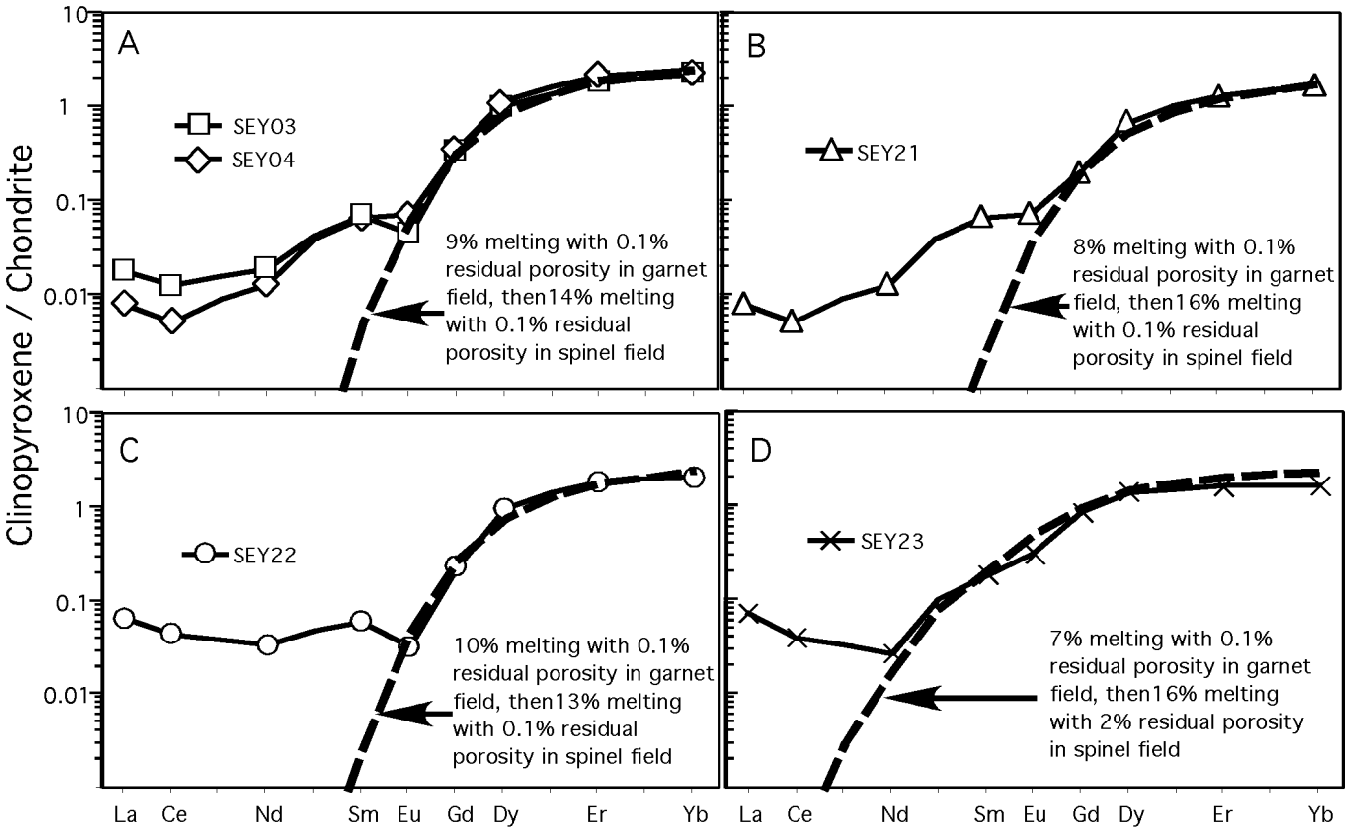

table

Click here to download table: Table01.rtf

Table 1 Sample numbers and their position in Hole 1274A cores.

Hole 1274A Sample#	core	section	interval	piece
SEY01	1R	1	4-5 cm	1
SEY02	1R	1	27-31 cm	4
SEY03	1R	1	65-66 cm	8
SEY04	1R	1	88-90 cm	10
SEY05	2R	1	33-36 cm	6
SEY06	3R	1	44-45 cm	6
SEY07	3R	1	85-86 cm	9
SEY08	4R	1	15-18 cm	1B
SEY09	4R	1	44-46 cm	2B
SEY10	4R	2	1-3 cm	1
SEY11	5R	1	3-5 cm	1
SEY12	5R	1	45-49 cm	7
HJBD01	6R	1	38-48 cm	6
HJBD02	6R	3	40-50 cm	1B
SEY13	7R	1	48-50 cm	4
HJBD03	7R	2	20-30 cm	2A
SEY14	8R	1	40-43 cm	7
HJBD04	8R	1	46-52 cm	8
SEY15	8R	2	9-11 cm	1
HJBD05	9R	1	14-16 cm	3
SEY16	11R	1	11-13 cm	2
HJBD06	11R	1	117-121 cm	17
SEY17	12R	1	2-4 cm	1
SEY18	12R	1	65-67 cm	10
SEY19	12R	1	72-75 cm	10
SEY20	12R	2	10-14 cm	3
HJBD07	13R	1	81-85 cm	9
HJBD08	14R	1	102-106 cm	12
SEY21	18R	1	13-16 cm	3
SEY22	18R	1	112-113 cm	19
HJBD09	19R	1	17-22 cm	4
HJBD10	20R	1	18-24 cm	4
HJBD11	23R	1	53-57 cm	11
HJBD12	24R	1	90-95 cm	5
HJBD13	26R	1	52-56 cm	9
SEY23	27R	1	87-90 cm	7
SEY24	27R	1	112-116 cm	8
SEY25	27R	2	18-21 cm	2

table

Click here to download table: Table02.rtf

Table 2 Reconstructed primary modal compositions (vol%) of representative ODP Leg 209 Hole peridotites.

	Li	Ol	Opx	Tot. Cpx	Tot. Sp	Cpx*	S1
SEY02	H	81.1	17.6	0.71	0.57	0.36	0.58
SEY03	H	72.3	24.2	2.30	1.24	1.56	1.22
SEY04	L	77.2	17.1	4.72	0.51	3.48	2.07
SEY07	H	74.2	23.7	1.57	0.57	0.87	1.17
SEY11	H	77.1	19.9	2.20	0.80	1.09	1.84
SEY14	H	70.3	27.2	2.06	0.49	1.32	1.23
SEY15	D	96.2	0.1	2.2	1.5	1.2	1.5
SEY16	H	72.8	25.1	1.68	0.45	1.02	1.10
SEY21	H	74.1	22.0	2.58	1.27	1.56	1.70
SEY22	H	80.5	16.8	1.82	0.80	1.21	1.01
SEY23	H	84.1	13.4	1.74	0.77	1.18	0.94
SEY25	H	77.3	19.9	1.99	0.75	0.86	1.88

Sample composition is represented by a single, standard-sized, thin section (~6000 points). Li, Lithology: H, harzburgite, L, lherzolite, D, dunite. Mineral abbreviations: Ol, olivine; Opx, orthopyroxene; Tot. Cpx, total clinopyroxene; Tot. Sp, total spinel; Cpx*, interstitial clinopyroxene grains not intergrown with spinel, and selvages on orthopyroxenes; S1, Type 1 clinopyroxene-spinel symplectites.

Table 3 Average major element compositions (in wt%) of olivines of ODP Leg 209 Site 1274A peridotites.

	Li	n	SiO_2	1σ	FeO	1σ	MnO	1σ	NiO	1σ	MgO	1σ	CaO	1σ	Total	1σ	MG#	1σ
SEY01	H	9	41,07	5	8,55	16	0,10	1	0,37	3	49,66	11	0,08	1	98,44	9	0,9119	16
SEY02	H	9	41,14	18	8,78	17	0,11	1	0,40	1	49,97	32	0,04	2	99,02	55	0,9103	15
SEY03	H	10	41,15	13	8,70	13	0,12	2	0,39	1	50,33	8	0,07	2	99,33	22	0,9115	13
SEY04	L	10	41,06	37	8,52	36	0,13	1	0,38	2	49,72	97	0,07	2	99,34	105	0,9123	26
SEY05	H	7	40,76	58	8,75	18	0,12	3	0,39	2	49,50	8	0,08	2	98,92	93	0,9098	15
SEY06	H	3	40,80	2	8,56	5	0,13	1	0,37	2	49,76	13	0,06	1	98,68	21	0,9120	3
SEY07	H	10	41,28	25	8,83	9	0,14	2	0,42	2	50,26	22	0,06	2	99,55	48	0,9103	9
SEY08	H	10	40,77	15	8,84	12	0,12	2	0,39	2	49,24	27	0,07	1	98,89	25	0,9084	14
SEY09	H	7	41,15	16	8,80	11	0,13	1	0,43	3	49,96	12	0,06	1	100,24	28	0,9100	10
SEY10	H	6	41,23	13	8,82	7	0,13	1	0,40	2	49,70	18	0,07	1	99,96	25	0,9094	6
SEY11	H	6	40,46	29	8,23	7	0,11	2	0,37	2	49,18	18	0,04	1	97,43	32	0,9142	9
SEY12	H	9	41,41	30	8,78	13	0,12	2	0,39	2	50,66	91	0,07	2	100,71	106	0,9114	22
HJBD01	H	6	40,64	17	8,29	26	0,10	1	0,35	4	50,40	13	0,08	1	99,89	23	0,9155	25
HJBD02	H	6	40,73	13	8,60	16	0,10	2	0,39	2	49,94	20	0,08	1	99,89	37	0,9118	14
SEY13	H	6	41,35	44	8,63	9	0,14	1	0,43	3	50,24	22	0,07	1	99,42	66	0,9121	9
HJBD03	H	5	40,50	30	8,50	10	0,11	2	0,38	3	49,88	16	0,07	2	99,46	43	0,9127	7
SEY14	H	13	41,13	43	8,81	33	0,13	2	0,41	3	50,02	34	0,05	2	99,34	55	0,9100	33
HJBD04	H	6	40,66	13	8,51	11	0,10	2	0,39	2	49,95	6	0,09	1	99,70	6	0,9128	11
SEY15	D	12	40,81	19	8,55	10	0,12	2	0,36	2	49,85	31	0,22	1	98,91	28	0,9122	13
HJBD05	H	6	40,98	18	8,58	13	0,10	2	0,37	4	49,96	16	0,09	1	100,11	35	0,9121	12
SEY16	H	7	40,77	10	8,70	12	0,13	3	0,40	3	48,88	12	0,07	1	98,09	9	0,9092	13
HJBD06	H	6	41,19	17	8,31	15	0,11	2	0,37	4	50,36	10	0,08	0	100,43	26	0,9152	13
SEY17	H	7	41,21	14	8,74	6	0,13	2	0,42	2	49,74	11	0,06	1	100,11	19	0,9102	5
SEY18	H	11	41,09	442	8,40	97	0,12	2	0,37	11	47,87	472	0,24	65	98,06	42	0,9104	24
SEY19	H	2	41,17	16	8,62	11	0,15	1	0,41	0	49,98	16	0,05	1	99,37	15	0,9117	13
SEY20	H	4	40,65	44	8,79	5	0,13	1	0,41	3	50,93	41	0,05	2	99,70	11	0,9117	12
HJBD07	H	6	40,51	19	8,31	11	0,11	2	0,34	4	50,28	20	0,05	1	99,61	44	0,9152	9
HJBD08	H	6	40,57	18	8,22	25	0,11	2	0,32	2	50,07	8	0,04	1	99,35	31	0,9156	23
SEY21	H	3	41,04	21	8,56	13	0,11	3	0,42	5	50,43	2	0,06	1	99,61	30	0,9130	12
SEY22	H	8	41,07	23	8,73	16	0,13	2	0,40	3	50,03	23	0,06	2	99,84	37	0,9109	18
HJBD09	H	6	40,61	21	8,18	15	0,10	3	0,35	4	50,21	19	0,05	1	99,53	46	0,9162	14
HJBD10	H	6	40,53	11	8,24	12	0,11	1	0,34	4	50,46	13	0,06	1	99,77	22	0,9160	11
HJBD11	H	6	40,58	13	8,20	29	0,14	2	0,30	3	50,20	12	0,06	1	99,52	36	0,9160	26
HJBD12	H	6	40,86	16	8,17	14	0,10	3	0,30	3	50,56	15	0,06	1	100,07	19	0,9168	14
HJBD13	H	6	41,03	13	8,49	16	0,10	3	0,34	3	50,52	20	0,06	1	100,56	38	0,9138	14
SEY23	H	7	41,18	22	8,61	18	0,12	2	0,41	2	49,61	33	0,07	2	99,27	31	0,9112	20
SEY24	H	5	41,00	19	8,73	11	0,14	1	0,43	1	49,37	48	0,06	1	98,74	48	0,9097	17
SEY25	H	3	41,20	11	8,68	12	0,11	0	0,40	3	50,53	5	0,05	1	99,97	17	0,9120	12
AVE.		111	40,93	32	8,56	17	0,12	2	0,38	3	49,95	34	0,07	3	99,44	36	0,9123	15

First column, sample numbers as in Table 1. Second column, Li, lithology: H, harzburgite; L, lherzolite; D, dunite. Third column, n, number of analyses. Columns next to oxide compositions give 1σ standard deviations in terms of the least unit cited: e.g. 41.07 (SiO_2) and 5 (1σ) represent 41.07 ± 0.05. Mg#, molar Mg/(Mg+Fe).

Electronic supplementary material

Table 4 Average major element compositions (in wt%) of orthopyroxenes of ODP Leg 209 Hole 1274A peridotites.

	Li	Type	n	SiO_2	1σ	TiO_2	1σ	Al_2O_3	1σ	Cr_2O_3	1σ	FeO	1σ	MnO	1σ	MgO	1σ	NiO	1σ	CaO	1σ	Na_2O	1σ	Total	1σ	MG#	1σ	CR#	1σ
SEY01	H	LPc	7	55,62	11	0,03	1	2,65	11	0,87	3	5,45	10	0,13	4	32,60	23	0,09	3	2,17	30	0,00	1	99,62	20	0,9142	12	0,1804	21
SEY02	H	LPc	17	55,03	15	0,03	1	3,59	10	1,01	8	5,69	11	0,13	2	32,27	23	0,10	2	1,84	33	0,01	1	99,68	22	0,9100	14	0,1583	78
SEY02	H	SPc	14	55,37	16	0,03	1	3,18	20	0,79	4	5,72	9	0,11	2	32,73	24	0,09	2	1,55	23	0,00	0	99,58	20	0,9107	14	0,1438	66
SEY02	H	Pr	3	55,52	22	0,03	0	3,18	20	0,76	6	5,76	6	0,10	2	32,84	35	0,09	4	1,51	27	0,01	1	99,81	14	0,9104	15	0,1389	37
SEY02	H	S	11	56,16	27	0,03	1	3,13	29	0,78	6	5,71	10	0,12	2	32,64	27	0,08	2	1,31	20	0,00	0	99,97	35	0,9107	15	0,1442	85
SEY03(1)	H	LPc	4	55,30	19	0,04	2	2,90	13	1,05	4	5,36	12	0,11	3	31,94	42	0,10	2	2,87	54	0,00	1	99,69	23	0,9139	11	0,1960	39
SEY03(1)	H	SPc	2	55,53	18	0,03	3	2,72	5	0,94	0	5,42	8	0,11	0	32,47	20	0,13	2	2,17	31	0,01	2	99,55	11	0,9143	7	0,1879	34
SEY03(1)	H	Pr	2	55,98	62	0,04	0	2,46	56	0,81	18	5,58	5	0,11	0	33,11	62	0,09	2	1,61	37	0,01	2	99,80	17	0,9136	7	0,1803	12
SEY04(1)	L	LPc	16	55,61	16	0,03	2	2,59	8	0,91	7	5,49	14	0,13	1	32,64	42	0,10	3	2,06	58	0,01	1	99,57	19	0,9137	13	0,1915	85
SEY04(1)	L	SPc	1	55,90		0,03		2,28		0,78		5,51		0,15		32,99		0,08		1,79		0,01		99,50		0,9144		0,1872	
SEY04(1)	L	Pr	2	55,61	19	0,03	1	2,74	10	0,94	17	5,51	3	0,17	1	32,98	6	0,11	1	1,50	17	0,00	0	99,58	9	0,9142	5	0,1861	215
SEY04(1)	L	S	1	56,09		0,03		2,51		0,82		5,56		0,13		32,81		0,08		1,48		0,00		99,52		0,9131		0,1801	
SEY05	H	LPc	1	55,27		0,04		3,30		1,01		5,99		0,10		32,27		0,11		1,89		0,01		99,98		0,9057		0,1697	
SEY05	H	SPc	8	55,25	18	0,04	1	3,09	11	0,91	4	6,09	7	0,13	3	32,28	12	0,09	2	1,65	18	0,01	1	99,54	22	0,9043	11	0,1651	26
SEY06	H	LPc	3	55,31	17	0,02	2	2,96	7	0,99	3	5,41	6	0,16	2	31,93	46	0,07	1	2,75	52	0,01	0	99,62	17	0,9131	9	0,1832	8
SEY07	H	LPc	9	55,58	18	0,02	1	2,85	13	0,92	9	5,68	13	0,14	3	32,64	46	0,11	3	1,82	54	0,00	0	99,77	18	0,9110	14	0,1775	95
SEY07	H	Pr	1	55,81		0,02		2,66		0,74		5,69		0,13		33,12		0,07		1,47		0,00		99,72		0,9121		0,1576	
SEY07	H	S	2	56,79	43	0,01	0	2,40	32	0,72	5	5,70	6	0,13	1	33,17	63	0,09	2	1,48	64	0,00	0	100,49	12	0,9121	6	0,1690	90
SEY08	H	SPc	11	55,57	18	0,02	1	2,72	11	0,92	5	5,70	7	0,13	2	32,64	17	0,11	3	1,79	21	0,02	2	99,62	22	0,9108	8	0,1851	33
SEY08	H	Pr	2	55,50	4	0,03	2	2,57	1	0,92	1	5,87	13	0,14	1	32,83	3	0,08	1	1,28	0	0,02	3	99,24	9	0,9089	20	0,1945	22
SEY08	H	S	1	56,75		0,02		2,27		0,70		5,69		0,13		33,21		0,07		1,10		0,00		99,94		0,9123		0,1718	
SEY09	H	SPc	8	55,63	13	0,03	1	2,76	12	0,90	6	5,83	4	0,14	2	32,51	18	0,10	2	1,93	18	0,01	1	99,82	16	0,9086	4	0,1795	59
SEY09	H	Pr	1	55,96		0,02		2,67		0,74		5,95		0,15		33,08		0,08		1,35		0,00		100,00		0,9083		0,1571	
SEY10	H	LPc	6	55,39	13	0,03	1	2,90	3	1,09	1	5,50	10	0,12	2	32,31	54	0,10	3	2,27	72	0,01	1	99,72	8	0,9128	9	0,2010	29
SEY10	H	SPc	7	55,53	16	0,03	1	2,71	7	0,92	4	5,78	10	0,13	2	32,43	21	0,10	2	1,99	30	0,01	1	99,63	19	0,9090	11	0,1858	69
SEY11	H	LPc	7	55,67	21	0,02	1	2,70	13	0,89	5	5,48	6	0,14	1	32,96	41	0,09	2	1,61	45	0,00	0	99,57	14	0,9147	10	0,1815	59
SEY11	H	SPc	2	56,01	75	0,02	0	2,65	13	0,85	3	5,40	6	0,14	1	32,73	20	0,11	4	1,65	51	0,00	0	99,56	19	0,9153	13	0,1776	15
SEY11	H	Pr	3	55,78	17	0,03	1	2,48	36	0,74	10	5,48	3	0,13	1	33,24	12	0,10	3	1,44	19	0,00	0	99,41	12	0,9153	4	0,1670	91
SEY12	H	LPc	13	55,21	15	0,04	1	3,26	5	1,01	3	5,76	11	0,13	2	32,08	30	0,11	3	2,13	44	0,03	1	99,74	24	0,9085	14	0,1723	53
SEY12	H	SPc	7	55,27	15	0,05	1	3,11	17	0,93	5	5,76	17	0,12	1	32,31	25	0,09	3	1,97	42	0,01	1	99,63	24	0,9091	23	0,1671	30
SEY12	H	Pr	7	55,59	51	0,04	1	2,81	66	0,79	17	5,93	15	0,14	2	32,80	42	0,11	2	1,43	21	0,01	1	99,65	13	0,9078	26	0,1592	48
HJBD01	H	LPc	10	56,05	14	0,02	1	2,54	5	0,91	4	5,34	11	0,13	2	32,69	29			2,44	41	0,00	0	100,12	38	0,9161	13	0,1936	53
HJBD02	H	LPc	10	56,15	17	0,01	1	2,72	10	1,02	4	5,33	30	0,14	2	32,27	47			2,80	57	0,00	0	100,43	22	0,9153	34	0,2011	49
SEY13	H	LPc	4	55,92	13	0,02	1	2,30	2	0,94	2	5,64	9	0,12	3	32,83	44	0,11	2	1,91	66	0,01	1	99,79	24	0,9121	4	0,2149	35
SEY13	H	SPc	7	55,97	14	0,01	1	2,17	7	0,84	5	5,63	5	0,14	1	32,94	17	0,11	2	1,82	20	0,00	0	99,63	20	0,9125	7	0,2057	78
HJBD03	H	SPc	10	56,01	20	0,01	1	2,62	13	0,93	4	5,34	16	0,15	2	32,52	51			2,43	87	0,00	0	99,99	31	0,9157	17	0,1925	59
HJBD03	H	Pr	10	56,14	30	0,00	1	2,47	17	0,77	5	5,69	15	0,15	3	33,28	15			1,67	4	0,00	0	100,17	14	0,9125	19	0,1722	56
SEY14	H	LPc	12	55,20	12	0,04	1	3,20	7	1,01	2	5,82	13	0,13	2	32,11	36	0,10	2	2,06	56	0,02	1	99,69	17	0,9077	14	0,1744	35
SEY14	H	SPc	20	55,62	20	0,03	1	2,77	21	0,88	6	5,84	12	0,13	2	32,66	34	0,10	1	1,68	46	0,01	1	99,73	18	0,9088	10	0,1758	69
SEY14	H	Pr	7	55,64	24	0,03	1	2,73	27	0,85	10	5,90	13	0,13	2	32,74	30	0,10	2	1,58	26	0,02	1	99,73	14	0,9082	16	0,1733	126
HJBD04	H	LPc	10	56,01	10	0,01	1	2,66	2	0,88	2	5,50	11	0,14	1	33,02	26			2,16	40	0,00	0	100,39	29	0,9145	14	0,1821	32
HJBD04	H	Pr	10	56,09	19	0,01	1	2,69	6	0,88	3	5,50	16	0,13	3	32,81	13			2,04	13	0,00	0	100,16	38	0,9140	20	0,1804	48
SEY15	D	S	2	56,25	25	0,03	1	1,95	15	0,73	6	5,39	3	0,12	1	32,56	22	0,08	2	2,24	34	0,01	1	99,37	25	0,9150	6	0,2016	49
HJBD05	H	LPc	10	56,32	12	0,01	1	2,80	6	1,03	3	5,45	12	0,12	2	32,44	22			2,41	35	0,00	0	100,58	14	0,9139	14	0,1973	58
HJBD05	H	Pr	9	55,98	44	0,01	1	2,80	6	1,01	6	5,50	11	0,14	3	32,34	41			2,47	59	0,00	0	100,26	44	0,9130	15	0,1953	73
SEY16	H	LPc	6	55,45	14	0,03	1	2,79	3	0,94	5	5,72	15	0,14	2	32,55	39	0,09	3	1,82	65	0,01	1	99,52	29	0,9103	16	0,1843	75
HJBD06	H	SPc	9	56,47	24	0,01	1	2,94	10	1,00	4	5,38	16	0,12	2	32,56	49			2,39	64	0,00	1	100,87	17	0,9152	17	0,1863	59
HJBD06	H	Pr	10	56,51	27	0,02	1	2,84	10	0,86	4	5,40	17	0,13	3	32,79	21			1,94	28	0,00	0	100,49	38	0,9155	25	0,1685	39
SEY17	H	LPc	14	55,46	14	0,02	1	2,81	6	0,97	3	5,69	12	0,14	2	32,40	26	0,10	2	2,04	34	0,01	1	99,65	22	0,9103	17	0,1886	52
SEY17	H	S	3	57,29	20	0,03	1	2,42	11	0,81	5	6,00	10	0,14	0	33,19	5	0,10	1	1,18	5	0,00	1	101,17	7	0,9078	15	0,1834	154
SEY18	H	LPc	12	55,89	36	0,03	1	2,58	30	0,89	6	5,63	11	0,14	3	32,72	27	0,10	2	1,62	41	0,01	1	99,62	25	0,9119	17	0,1890	84
SEY18	H	SPc	1	55,99		0,03		2,34		0,90		5,60		0,17		32,67		0,10		2,27		0,00		100,07		0,9123		0,2052	
SEY18	H	Pr	5	56,43	40	0,04	1	1,90	45	0,54	22	5,66	18	0,14	2	33,71	48	0,10	1	1,19	53	0,01	0	99,70	19	0,9139	23	0,1588	313
SEY19	H	LPc	3	56,17	17	0,03	0	2,43	7	0,85	4	5,57	10	0,14	1	33,45	21	0,11	3	1,03	38	0,01	1	99,80	9	0,9146	10	0,1906	93
SEY20	H	LPc	10	55,35	31	0,04	1	2,98	20	0,95	6	5,73	16	0,15	2	32,44	38	0,10	4	1,92	81	0,05	5	99,72	11	0,9099	16	0,1771	132
SEY20	H	Pr	1	55,83		0,05		2,61		0,72		5,89		0,11		33,31		0,11		1,05		0,01		99,68		0,9097		0,1554	
HJBD07	H	SPc	10	55,64	13	0,01	1	2,87	7	0,92	2	5,36	18	0,08	2	32,62	55			2,31	79	0,00	1	99,81	29	0,9157	16	0,1778	39
HJBD07	H	Pr	10	55,64	22	0,01	1	2,68	7	0,82	3	5,40	17	0,08	2	33,06	63			2,13	91	0,00	1	99,82	18	0,9161	15	0,1696	41
HJBD08	H	SPc	10	55,76	21	0,02	1	2,58	10	0,85	4	5,36	8	0,07	2	32,68	39			2,13	43	0,00	0	99,45	15	0,9158	11	0,1804	45
HJBD08	H	Pr	10	56,00	12	0,02	1	2,36	10	0,71	7	5,50	15	0,08	2	33,40	23			1,72	30	0,00	0	99,80	32	0,9154	17	0,1677	94
SEY21	H	S	3	56,42	30	0,04	1	2,94	10	0,87	1	5,59	18	0,12	1	32,89	25	0,10	1	1,76	31	0,02	1	100,75	52	0,9129	21	0,1655	34
SEY22	H	LPc	3	55,29	13	0,04	1	2,93	6	0,98	3	5,71	3	0,15	2	32,61	21	0,09	2	1,66	29	0,00	0	99,46	23	0,9106	1	0,1826	19
SEY22	H	Pr	2	55,68	1	0,03	0	2,65	12	0,86	4	5,67	11	0,17	4	32,73	7	0,10	3	1,72	4	0,02	2	99,63	10	0,9114	17	0,1791	128
HJBD09	H	LPc	9	55,47	18	0,00	0	2,89	5	0,95	3	5,38	18	0,08	2	32,57	29			2,24	38	0,01	1	99,59	35	0,9153	22	0,1806	45
HJBD09	H	Pr	10	55,84	18	0,00	0	2,75	9	0,81	4	5,37	13	0,08	2	32,54	38			2,58	59	0,01	1	99,97	33	0,9153	12	0,1652	31
HJBD10	H	LPc	10	55,30	16	0,00	0	2,92	7	0,97	2	5,38	15	0,09	2	32,75	22			2,06	17	0,01	1	99,48	31	0,9156	18	0,1826	26
HJBD10	H	Pr	8	55,71	29	0,00	0	2,70	3	0,74	2	5,40	16	0,09	3	33,24	16			1,63	6	0,00	0	99,51	50	0,9165	19	0,1555	35
HJBD11	H	LPc	10	55,75	27	0,02	1	2,88	10	0,92	3	5,36	15	0,14	2	32,68	32			2,46	42	0,02	2	100,23	51	0,9158	22	0,1762	50
HJBD11	H	Pr	10	55,96	25	0,02	1	2,64	9	0,84	3	5,40	13	0,12	1	33,09	17			1,95	19	0,02	2	100,04	27	0,9161	17	0,1755	44
HJBD12	H	LPc	10	55,80	13	0,02	1	2,26	10	0,90	2	5,26	17	0,12	2	32,78	35			2,43	43	0,02	1	99,60	38	0,9174	21	0,2110	53
HJBD12	H	Pr	10	55,62	55	0,02	1	2,31	7	0,84	3	5,41	21	0,12	2	32,94	34			2,20	33	0,03	2	99,49	61	0,9156	32	0,1969	68
HJBD13	H	SPc	10	56,42	24	0,06	1	2,24	7	0,84	3	5,27	10	0,12	1	32,97	26			2,12	28	0,10	2	100,13	36	0,9177	12	0,2022	62
HJBD13	H	Pr	11	56,33	13	0,05	1	2,46	4	0,94	3	5,45	11	0,11	1	32,85	13			2,00	22	0,07	3	100,25	23	0,9148	14	0,2041	45
SEY23(1)	H	LPc	8	55,54	11	0,06	1	2,82	6	1,04	2	5,53	12	0,12	2	32,56	31	0,11	2	1,97	38	0,04	1	99,77	13	0,9130	11	0,1981	27
SEY23(1)	H	SPc	9	55,65	25	0,05	2	2,77	8	0,89	6	5,65	10	0,13	2	32,52	28	0,09	2	1,96	40	0,08	4	99,79	23	0,9112	9	0,1778	84
SEY23(2)	H	S	2	57,34	5	0,04	0	2,12	17	0,63	4	5,68	11	0,15	2	33,18	7	0,09	1	1,26	10	0,02	0	100,51	26	0,9124	14	0,1670	25
SEY24	H	LPc	6	55,91	16	0,02	1	2,28	6	0,93	2	5,61	7	0,13	1	32,87	23	0,10	1	1,83	24	0,01	1	99,69	21	0,9125	9	0,2161	58
SEY24	H	SPc	13	56,13	31	0,01	1	2,26	7	0,88	5	5,67	11	0,14	3	32,35	38	0,10	3	2,02	51	0,02	1	99,58	17	0,9104	17	0,2063	62
SEY24	H	Pr	1	56,11		0,02		2,12		0,79		5,88		0,18		33,08		0,10		1,51		0,01		99,80		0,9092		0,1997	
SEY25	H	LPc	11	55,43	8	0,06	1	2,90	5	1,07	3	5,54	10	0,11	3	32,43	30	0,11	2	2,03	39	0,05	1	99,72	11	0,9126	11	0,1985	43
SEY25	H	SPc	3	55,68	18	0,05	1	2,82	6	0,94	5	5,56	6	0,11	2	32,97	89	0,10	2	1,43	97	0,05	3	99,72	13	0,9136	14	0,1823	68

The number in parentheses after sample numbers in the first column corresponds to thin section number, when two sections were analyzed in same sample. Orthopyroxene textural type: LPc, large (≥ 5 mm) porphyroclast cores; SPc, small (< 5 mm) porphyroclast cores; Pr, porphyroclast rims; S, intergrown with spinel. Cr#: molar Cr/(Cr+Al). Other abbreviations and column contents as in Table 3.

Table 5 Average major element compositions (in wt%) of clinopyroxenes of ODP Leg 209 Hole 1274A peridotites.

	Li	Type	n	SiO_2	1σ	TiO_2	1σ	Al_2O_3	1σ	Cr_2O_3	1σ	FeO	1σ	MnO	1σ	MgO	1σ	NiO	1σ	CaO	1σ	Na_2O	1σ	Total	1σ	MG#	1σ	CR#	1σ
SEY01	H	S	5	52,73	26	0,06	1	2,95	28	1,22	9	2,43	24	0,10	2	17,70	38	0,07	2	22,42	50	0,06	2	99,72	20	0,9287	53	0,2171	36
SEY02	H	S	3	53,04	27	0,07	1	2,63	47	0,85	12	2,22	9	0,10	0	17,54	12	0,04	1	23,05	4	0,08	2	99,83	11	0,9338	21	0,1795	59
SEY03(1)	H	IG/Gc	2	52,66	13	0,05	2	3,26	16	1,35	4	2,57	8	0,06	0	18,15	29	0,04	2	21,63	54	0,06	2	99,75	27	0,9263	12	0,2178	30
SEY03(1)	H	IGr	3	52,79	23	0,05	1	3,16	21	1,31	9	2,74	30	0,07	2	18,70	98	0,05	2	20,84	141	0,06	1	99,70	21	0,9241	39	0,2173	23
SEY03(1)	H	S	5	53,32	30	0,06	1	2,65	20	1,15	9	2,41	13	0,09	1	18,12	48	0,06	1	22,45	50	0,04	4	99,82	55	0,9306	19	0,2259	210
SEY03(2)	H	Gc	6	51,99	66	0,05	1	3,15	6	1,27	3	2,54	22	0,10	1	18,01	104	0,06	2	21,50	120	0,08	1	98,75	73	0,9275	21	0,2135	30
SEY03(2)	H	Gr	1	51,72		0,05		2,84		1,03		2,36		0,07		17,83		0,06		22,62		0,08		98,69		0,9316		0,1957	
SEY03(2)	H	IG	2	52,61	79	0,04	2	2,58	36	0,98	20	2,43	9	0,09	2	18,12	82	0,04	2	22,38	44	0,07	1	99,84	3	0,9306	6	0,2031	101
SEY04(1)	L	Pc	14	52,75	55	0,04	1	3,35	46	1,41	24	2,61	17	0,10	1	18,11	58	0,05	2	21,66	80	0,07	3	99,45	55	0,9252	34	0,2199	71
SEY04(1)	L	Pr	4	53,09	23	0,04	2	2,83	33	1,13	18	2,67	42	0,10	4	18,04	13	0,07	1	21,95	61	0,07	7	99,28	76	0,9235	106	0,2102	89
SEY04(1)	L	IG/G	2	52,90	18	0,04	1	2,99	29	1,16	16	2,49	18	0,09	1	18,10	27	0,07	0	21,90	74	0,07	2	99,41	28	0,9283	39	0,2065	67
SEY04(1)	L	S	2	52,64	119	0,04	1	2,63	24	1,16	2	2,44	16	0,09	3	17,51	84	0,05	2	22,45	14	0,08	2	99,80	19	0,9275	11	0,2290	132
SEY04(2)	L	Pc	10	51,36	59	0,04	2	3,36	15	1,42	8	2,56	12	0,10	2	17,80	47	0,06	1	22,02	59	0,06	2	98,83	68	0,9261	22	0,2209	48
SEY04(2)	L	Pr	8	51,67	65	0,04	0	3,01	20	1,22	10	2,48	10	0,10	0	17,92	30	0,06	0	22,42	40	0,06	0	98,98	100	0,9286	24	0,2135	68
SEY04(2)	L	IG/G	2	50,59	12	0,04	0	3,28	6	1,39	9	2,41	23	0,11	1	17,88	12	0,07	1	22,06	81	0,08	1	97,93	77	0,9304	66	0,2217	135
SEY05	H	S	6	52,65	34	0,07	1	3,40	16	1,21	10	2,70	13	0,08	2	17,35	30	0,05	2	22,15	28	0,19	5	100,20	62	0,9197	31	0,1932	148
SEY06	H	IG	2	52,98	56	0,05	1	3,21	49	1,19	17	2,46	40	0,10	2	17,83	60	0,05	0	22,37	69	0,07	1	98,60	102	0,9283	87	0,1997	13
SEY06	H	S	1	52,72		0,05		2,70		1,15		2,14		0,08		17,19		0,07		23,34		0,06		98,71		0,9346		0,2226	
SEY07	H	S	6	52,76	19	0,04	0	3,24	22	1,27	7	2,54	16	0,09	3	18,09	35	0,06	2	21,86	57	0,06	1	100,66	27	0,9270	34	0,2084	117
SEY07	H	IG	4	52,59	16	0,05	0	3,27	28	1,23	14	2,48	27	0,09	2	17,55	42	0,06	2	22,44	80	0,06	1	100,63	28	0,9266	58	0,2014	60
SEY08	H	S	9	52,73	31	0,04	1	3,12	26	1,23	8	2,65	21	0,09	3	17,81	47	0,05	2	21,87	65	0,11	7	99,89	42	0,9231	53	0,2100	58
SEY09	H	IG	3	52,79	32	0,03	1	3,07	52	1,16	23	2,65	16	0,10	1	17,70	48	0,08	2	22,11	62	0,10	2	99,78	21	0,9224	37	0,2008	65
SEY09	H	S	6	52,74	19	0,04	1	3,09	18	1,28	5	2,69	20	0,09	2	17,84	53	0,06	2	21,90	79	0,08	1	99,83	9	0,9221	35	0,2180	88
SEY10	H	Gc	2	52,70	3	0,04	1	3,13	8	1,30	0	2,76	48	0,08	3	18,05	113	0,08	1	21,46	183	0,09	3	99,69	10	0,9213	81	0,2175	39
SEY10	H	S	6	52,80	27	0,04	1	2,90	23	1,27	7	2,60	14	0,10	2	17,66	52	0,05	2	22,24	60	0,09	4	99,74	21	0,9238	26	0,2276	152
SEY11	H	Gc	10	52,74	28	0,03	1	3,20	16	1,25	4	2,65	32	0,09	3	18,54	88	0,06	2	21,05	129	0,05	1	99,67	22	0,9258	58	0,2072	71
SEY11	H	Gr	2	52,67	8	0,02	1	3,48	3	1,26	4	2,69	13	0,10	1	18,87	56	0,06	3	20,48	76	0,05	1	99,69	2	0,9259	13	0,1960	60
SEY11	H	IG	3	53,46	83	0,03	2	2,43	81	0,82	40	2,25	24	0,09	3	18,77	89	0,06	1	21,76	102	0,05	1	99,72	4	0,9368	77	0,1798	288
SEY11	H	S	3	52,80	30	0,03	0	3,09	39	1,23	18	2,68	11	0,09	1	18,74	46	0,05	2	20,84	42	0,05	0	99,57	16	0,9257	12	0,2100	61
SEY12	H	S	7	52,41	23	0,08	2	3,56	34	1,29	12	2,81	14	0,09	1	17,81	63	0,06	3	21,54	86	0,11	1	99,75	7	0,9185	31	0,1952	109
HJBD01	H	IG	7	52,95	42	0,05	1	3,01	11	1,22	5	2,28	9	0,10	2	17,95	57			22,78	54	0,12	4	100,46	48	0,9334	19	0,2143	53
HJBD02	H	IG	10	52,88	49	0,03	1	3,26	15	1,33	6	2,69	19	0,10	2	18,29	74			21,82	102	0,04	2	100,46	54	0,9237	23	0,2149	49
SEY13	H	IG	3	53,00	17	0,02	1	2,58	10	1,16	4	2,67	25	0,08	3	18,14	80	0,05	1	21,94	112	0,04	1	99,68	12	0,9238	37	0,2310	24
HJBD03	H	Gc	10	53,11	55	0,03	1	3,48	11	1,48	9	3,26	66	0,10	3	20,27	280			18,86	390	0,02	3	100,60	26	0,9171	44	0,2218	62
HJBD03	H	Gr	10	52,72	69	0,02	1	3,16	13	1,32	8	2,75	26	0,10	3	18,72	98			21,35	143	0,01	2	100,15	61	0,9239	39	0,2185	70
SEY14	H	IG/Gc	3	52,61	5	0,04	0	3,26	22	1,44	11	2,63	22	0,08	1	17,86	88	0,04	1	21,96	124	0,05	2	99,97	21	0,9238	28	0,2283	220
SEY14	H	IG/Gr	6	52,82	47	0,04	1	2,86	55	1,18	31	2,57	20	0,08	1	17,71	44	0,05	2	22,44	68	0,04	2	99,80	11	0,9248	48	0,2154	243
SEY14	H	S	1	52,36		0,05		3,25		1,33		2,55		0,06		17,18		0,06		22,71		0,07		99,62		0,9233		0,2153	
HJBD04	H	IG/Gc	7	50,87	40	0,03	1	3,32	10	1,34	5	3,00	14	0,12	2	19,22	50			20,60	68	0,04	3	98,53	50	0,9195	20	0,2138	69
HJBD04	H	IG/Gr	9	52,36	37	0,04	1	3,34	6	1,28	3	2,53	15	0,10	2	17,70	34			22,71	49	0,05	1	100,10	36	0,9259	31	0,2040	12
SEY15	D	IG	1	53,24		0,05		2,46		1,12		2,33		0,10		18,02		0,05		22,17		0,14		99,68		0,9324		0,2347	
SEY15	D	S	3	52,81	46	0,07	1	2,88	44	1,27	17	2,20	29	0,06	5	17,46	23	0,04	3	22,81	85	0,12	2	99,72	19	0,9340	76	0,2286	62
HJBD05	H	IGc	5	51,44	40	0,04	1	3,23	6	1,34	3	2,85	16	0,10	2	19,27	43			20,68	62	0,08	3	99,03	53	0,9234	35	0,2175	28
HJBD05	H	IGr	10	52,89	57	0,05	1	3,26	9	1,31	5	2,50	16	0,10	2	18,44	58			21,79	87	0,11	3	100,45	48	0,9294	23	0,2127	41
SEY16	H	IG	5	52,56	31	0,04	1	3,16	22	1,26	14	2,25	10	0,07	1	17,12	18	0,05	1	23,05	17	0,09	2	99,63	21	0,9313	32	0,2107	76
SEY16	H	S	9	52,82	32	0,03	1	2,81	49	1,21	12	2,23	17	0,08	2	17,36	24	0,06	3	23,05	36	0,08	1	99,73	21	0,9327	49	0,2271	190
HJBD06	H	IGc	8	52,20	90	0,04	1	3,38	10	1,37	6	2,49	20	0,11	2	18,99	86			20,89	130	0,05	2	99,51	68	0,9314	27	0,2137	82
HJBD06	H	IGr	8	53,27	97	0,05	1	3,01	44	1,15	18	2,21	17	0,09	2	18,08	79			22,68	120	0,04	2	100,58	111	0,9359	29	0,2039	40
SEY17	H	S	2	52,75	15	0,02	0	3,27	4	1,33	2	2,90	0	0,12	3	18,56	6	0,06	1	20,73	5	0,08	0	99,83	21	0,9195	2	0,2138	45
SEY18	H	Gc	8	52,75	27	0,07	1	3,13	35	1,33	15	2,39	31	0,09	2	18,19	69	0,05	2	21,68	118	0,09	1	99,77	16	0,9314	70	0,2212	48
SEY18	H	Gr	4	52,86	51	0,06	1	2,88	66	1,24	29	2,19	13	0,09	2	17,85	58	0,05	2	22,36	91	0,09	2	99,67	16	0,9356	40	0,2244	83
SEY18	H	IG	2	53,54	11	0,04	0	1,95	3	0,61	0	2,09	2	0,08	3	17,64	20	0,04	1	23,52	20	0,06	1	99,57	14	0,9376	1	0,1744	17
SEY18	H	S	7	53,45	46	0,07	2	2,08	49	0,85	27	2,08	7	0,07	3	17,76	44	0,06	1	23,18	58	0,09	2	99,70	20	0,9382	16	0,2122	184
SEY19	H	S	3	53,88	16	0,04	1	1,75	27	0,62	15	2,06	5	0,07	3	17,87	20	0,03	3	23,43	16	0,08	2	99,82	17	0,9392	15	0,1909	271
SEY20	H	G	4	52,71	19	0,08	1	3,08	40	1,23	15	2,22	39	0,09	1	17,73	94	0,06	2	22,52	175	0,07	1	99,79	17	0,9347	73	0,2119	65
SEY20	H	IG	1	53,16		0,09		2,44		0,79		2,31		0,06		17,77		0,04		23,00		0,05		99,71		0,9320		0,1789	
SEY20	H	S	5	52,66	29	0,08	2	2,99	34	1,23	17	2,10	17	0,07	1	17,34	44	0,05	3	23,10	57	0,08	2	99,71	16	0,9363	34	0,2161	68
HJBD07	H	IG	5	53,00	16	0,09	1	2,43	19	0,98	6	1,48	5	0,04	1	17,44	22			24,17	18	0,13	3	99,76	14	0,9545	14	0,2132	77
HJBD08	H	Gc	6	53,16	50	0,11	1	2,58	15	1,02	9	1,99	10	0,05	2	17,42	18			23,83	42	0,13	2	100,29	36	0,9399	31	0,2097	88
HJBD08	H	Gr	4	54,07	24	0,07	1	1,86	13	0,58	4	2,13	1	0,03	4	17,89	6			23,67	15	0,10	1	100,39	14	0,9375	4	0,1720	58
SEY21	H	S	9	52,74	34	0,05	3	3,29	26	1,28	10	2,54	35	0,08	2	18,00	62	0,05	2	21,12	100	0,24	9	99,39	30	0,9268	78	0,2078	77
SEY22	H	IG/Gc	1	52,60		0,07		3,46		1,33		2,36		0,08		17,18		0,04		22,46		0,23		99,80		0,9285		0,2045	
SEY22	H	IG	11	52,54	41	0,05	2	3,29	33	1,27	7	2,27	14	0,08	2	17,40	21	0,05	2	22,02	57	0,22	5	99,20	51	0,9317	38	0,2063	85
SEY22	H	Gr	2	52,26	17	0,03	0	3,26	5	1,18	0	2,21	8	0,05	3	17,26	28	0,06	1	22,19	15	0,19	1	98,68	13	0,9330	31	0,1952	21
SEY22	H	S	7	52,69	35	0,04	1	3,27	22	1,28	13	2,49	19	0,09	1	18,13	55	0,05	2	21,09	95	0,18	2	99,31	31	0,9286	30	0,2082	126
HJBD09	H	IG	9	52,70	35	0,04	1	3,07	10	1,16	4	2,08	8	0,05	2	17,58	35			23,11	31	0,22	3	100,01	36	0,9376	19	0,2021	50
HJBD10	H	IG	7	52,27	45	0,06	1	3,25	22	1,26	7	2,29	12	0,05	2	17,50	8			22,81	41	0,27	3	99,77	53	0,9315	34	0,2069	41
HJBD11	H	IG	10	52,73	49	0,06	1	3,02	23	1,20	10	2,40	17	0,09	2	17,90	55			22,90	65	0,20	3	100,50	40	0,9299	31	0,2096	57
HJBD12	H	IG/Gc	7	52,99	16	0,06	2	2,68	11	1,29	3	2,36	17	0,10	2	18,79	59			21,80	97	0,11	2	100,18	24	0,9341	24	0,2439	95
HJBD12	H	IG/Gr	10	52,96	13	0,06	1	2,62	15	1,20	10	2,33	9	0,10	2	18,53	34			22,21	55	0,11	2	100,12	25	0,9340	20	0,2351	70
HJBD13	H	IG	10	53,12	45	0,12	2	2,99	11	1,37	6	2,21	12	0,09	2	17,40	27			22,58	72	0,50	3	100,38	78	0,9334	27	0,2347	62
SEY23(1)	H	IG	11	53,10	40	0,07	1	3,10	33	1,32	12	2,12	12	0,06	2	16,94	33	0,04	2	21,89	61	0,57	7	99,21	43	0,9344	28	0,2225	70
SEY23(1)	H	S	3	53,22	20	0,08	1	2,90	33	1,31	24	2,24	25	0,08	1	16,85	15	0,04	1	22,50	61	0,54	6	99,77	18	0,9308	66	0,2317	243
SEY23(2)	H	IG	4	51,98	51	0,10	3	2,96	29	1,29	11	2,23	25	0,08	1	17,32	94	0,05	1	21,94	107	0,47	3	98,43	78	0,9333	39	0,2261	98
SEY24	H	S	1	53,06		0,02		2,72		1,13		2,52		0,10		17,88		0,03		22,39		0,04		99,90		0,9267		0,2173	
SEY25	H	IG	9	53,22	32	0,06	2	2,98	36	1,24	13	2,04	8	0,06	1	16,79	15	0,05	2	21,80	55	0,52	7	98,76	71	0,9363	26	0,2188	129
SEY25	H	S	7	52,94	46	0,05	1	2,59	35	1,19	10	1,94	16	0,06	2	17,06	16	0,04	2	21,94	31	0,45	2	98,27	33	0,9400	42	0,2362	152
AVE.			423	52,72	1	0,05	0	2,98	0	1,20	0	2,42	0	0,08	0	17,91	1	0,05	0	22,14	1	0,12	0	99,65	1	0,9296	62	0,2124	144

Clinopyroxene textural types: Pc and Pr, coarse (≥ 3 mm) grains in lherzolite sample, core and rim; Gc and Gr, medium (≥ 0.5 x ≥ 1 mm) grains, core and rim; IG, IGc, IGr, small (< 0.5 mm x 0.5-1 mm) interstitial grains and selvages on orthopyroxenes, whole grain, core and rim, respectively; S, in S1 and S2 symplectites and in opx-spinel clusters. Other abbreviations and column contents as in Table 3 and 4.

Electronic supplementary material

Table 6 Average major element compositions (in wt%) of spinels of ODP Leg 209 Hole 1274A peridotites.

	Li	n	SiO_2	1σ	TiO_2	1σ	Al_2O_3	1σ	Cr_2O_3	1σ	Fe_2O_3	1σ	FeO	1σ	MnO	1σ	MgO	1σ	NiO	1σ	Total	1σ	Cr#	1σ	Mg#	1σ
SEY01	H	4	0,05	1	0,05	1	30,26	64	41,10	120	0,02	1	13,16	53	0,21	3	15,43	38	0,11	2	100,39	41	0,4767	125	0,6764	142
SEY02	H	2	0,12	12	0,06	3	38,33	16	32,40	26	0,05	22	12,17	30	0,17	1	16,95	29	0,18	1	100,43	16	0,3618	28	0,7130	85
SEY03	H	2	0,11	9	0,07	1	29,64	47	42,00	109	0,24	26	13,29	14	0,16	2	15,53	0	0,12	2	101,16	14	0,4873	105	0,6757	23
SEY04	L	4	0,39	61	0,04	1	29,73	152	40,41	208	0,01	67	13,67	102	0,22	2	15,18	34	0,12	1	99,78	73	0,4769	244	0,6645	208
SEY05	H	5	0,04	1	0,06	1	34,22	277	35,73	335	1,19	18	12,64	59	0,16	4	16,14	59	0,17	2	100,34	61	0,4121	417	0,6947	173
SEY07	H	5	0,04	3	0,04	1	31,80	63	38,12	61	0,66	10	13,16	27	0,20	3	15,37	16	0,13	2	99,53	16	0,4457	87	0,6757	68
SEY08	H	5	0,04	1	0,04	1	28,88	95	41,07	96	1,13	7	13,85	10	0,20	2	14,75	12	0,11	1	100,07	42	0,4883	138	0,6552	15
SEY09	H	11	0,49	120	0,04	1	27,53	182	41,19	204	1,66	105	14,60	57	0,20	3	14,55	93	0,12	3	100,38	183	0,5011	215	0,6393	178
SEY10	H	5	0,07	1	0,05	1	29,59	56	41,20	48	1,18	5	13,46	23	0,21	2	15,32	15	0,14	1	101,22	42	0,4829	74	0,6699	56
SEY11	H	5	0,24	34	0,03	1	29,00	136	38,54	149	0,47	91	13,84	86	0,20	3	14,23	35	0,09	2	96,62	23	0,4714	215	0,6471	187
SEY12	H	5	0,32	60	0,07	0	33,04	43	37,51	18	0,48	27	14,39	46	0,19	2	15,38	43	0,14	2	101,51	86	0,4323	36	0,6559	55
HJBD01	H	6	0,10	1	0,05	1	29,54	31	41,73	17	0,45	41	12,97	57	0,20	3	15,57	31	0,14	2	100,76	37	0,4865	24	0,6815	139
HJBD02	H	6	0,07	1	0,05	1	29,38	54	42,01	35	0,24	25	13,94	16	0,21	2	14,91	8	0,15	1	100,97	25	0,4895	64	0,6558	32
SEY13	H	7	0,03	2	0,06	1	27,58	36	43,48	37	1,27	17	13,45	18	0,21	4	15,11	10	0,14	2	101,33	19	0,5139	52	0,6670	44
HJBD03	H	6	0,07	1	0,03	1	29,21	53	42,10	54	0,46	20	13,14	28	0,20	2	15,38	20	0,16	2	100,75	17	0,4914	76	0,6759	75
SEY14	H	9	0,05	2	0,10	4	28,65	52	42,50	78	0,66	38	14,52	63	0,21	2	14,59	43	0,12	3	101,41	44	0,4987	86	0,6417	168
HJBD04	H	6	0,07	1	0,04	2	31,30	48	39,07	74	1,26	15	13,59	20	0,17	3	15,36	12	0,19	2	101,05	34	0,4557	84	0,6682	48
SEY15	D	7	0,08	1	0,10	1	26,64	58	43,73	38	1,69	27	13,87	22	0,22	3	14,80	34	0,12	2	101,24	82	0,5240	67	0,6554	85
HJBD05	H	5	0,08	2	0,05	1	30,43	35	41,56	31	0,06	7	12,90	19	0,17	3	15,74	21	0,18	3	101,18	19	0,4781	46	0,6849	60
SEY16	H	4	0,04	1	0,03	1	30,35	28	40,81	34	0,30	16	14,50	29	0,20	3	14,68	21	0,11	2	101,03	21	0,4742	37	0,6435	78
HJBD06	H	6	0,07	3	0,05	1	31,07	80	41,20	90	0,08	8	13,20	19	0,17	2	15,73	15	0,18	4	101,75	35	0,4707	117	0,6798	45
SEY17	H	3	0,06	0	0,04	1	29,24	115	41,49	137	1,30	20	14,32	20	0,21	1	14,80	11	0,11	2	101,56	25	0,4876	180	0,6481	35
SEY18	H	4	0,10	2	0,08	1	28,78	88	41,95	101	0,04	5	14,31	28	0,19	3	14,53	22	0,10	1	100,07	14	0,4944	136	0,6443	80
SEY19	H	1	0,20		0,06		29,82		36,87		4,31		13,51		0,21		15,23		0,12		100,31		0,4533		0,6678	
SEY20	H	1	0,07		0,06		31,55		36,24		4,40		9,32		0,17		17,96		0,13		99,89		0,4351		0,7746	
HJBD07	H	6	0,06	2	0,12	2	31,48	42	39,82	45	0,55	23	12,53	10	0,21	3	16,12	12	0,13	3	101,02	38	0,4589	59	0,6963	31
HJBD08	H	6	0,09	1	0,13	1	31,63	97	38,57	127	0,58	31	13,77	39	0,21	2	15,21	28	0,12	3	100,33	43	0,4499	155	0,6631	100
SEY21	H	3	0,11	3	0,07	1	32,03	86	39,93	56	0,28	5	13,19	52	0,19	2	15,95	53	0,15	4	101,91	44	0,4554	99	0,6831	158
SEY22	H	5	0,10	1	0,05	1	30,80	197	39,94	151	1,03	7	13,19	17	0,23	1	15,62	50	0,14	1	101,10	115	0,4654	248	0,6784	95
HJBD09	H	6	0,11	5	0,10	1	32,35	18	38,68	16	0,52	7	12,25	6	0,19	2	16,37	7	0,14	4	100,70	17	0,4450	21	0,7042	16
HJBD10	H	6	0,08	2	0,11	1	31,99	31	39,09	45	0,49	23	12,47	14	0,19	3	16,18	11	0,13	3	100,72	12	0,4504	52	0,6981	36
HJBD11	H	6	0,04	1	0,05	1	32,68	34	37,93	31	0,87	13	12,91	13	0,19	3	15,89	7	0,12	2	100,69	26	0,4377	46	0,6869	28
HJBD12	H	5	0,05	1	0,10	1	28,03	9	43,28	10	0,71	9	13,35	12	0,19	2	15,24	5	0,10	3	101,06	21	0,5087	12	0,6705	26
HJBD13	H	6	0,12	2	0,10	1	30,63	43	40,61	42	0,23	27	14,12	35	0,19	1	15,08	15	0,09	3	101,24	24	0,4707	57	0,6555	77
SEY23	H	5	0,03	1	0,08	1	29,92	125	40,99	110	0,78	16	13,48	65	0,19	2	15,27	56	0,14	3	100,89	51	0,4790	167	0,6687	187
SEY25	H	5	0,11	3	0,07	2	30,66	89	40,39	145	0,12	17	14,53	34	0,20	3	14,76	23	0,11	2	100,95	56	0,4690	162	0,6442	90
AVE.		83	0,11	10	0,07	1	30,49	76	40,09	85	0,83	23	13,38	34	0,20	2	15,41	26	0,13	2	100,70	42	0,4689	110	0,6724	86

Fe_2O and Fe_2O_3 recalculated by stoichiometry. Mg# = $Mg/(Mg+Fe^{2+})$. Other abbreviations and column contents as in Table 3 and 4.

Electronic supplementary material

Table 7 Trace element (ppm) and Na_2O (wt%) compositions of representative clinopyroxenes from ODP Leg 209 Hole 1274A peridotites.

		Type	La	Ce	Sr	Nd	Zr	Sm	Eu	Gd	Ti	Tb	Dy	Er	Yb	Lu	Na_2O
SEY03(2)	cpx1	SLVc	0,005	0,007	0,755	0,016	0,080	0,012	0,004	0,057	334,4	0,022	0,253	0,273	0,387	0,052	0,08
SEY03(2)	cpx2	Gc	0,006	0,013	0,455	0,005	0,093	0,009	0,003	0,067	322,9	0,028	0,258	0,291	0,366	0,054	0,08
SEY03(2)	cpx3	Gr	0,002	0,003	0,723	0,005	0,064	0,008	0,001	0,069	292,0	0,023	0,208	0,267	0,333	0,059	0,03
SEY04(1)	cpx13	Pc	0,002	0,004	1,042	0,009	0,106	0,008	0,000	0,062	319,8	0,023	0,283	0,298	0,359	0,061	0,07
SEY04(1)	cpx14	Pr	0,004	0,003	0,452	0,008	0,121	0,008	0,004	0,063	318,6	0,028	0,310	0,308	0,428	0,060	0,07
SEY04(1)	cpx15	FC	0,006	0,007	0,733	0,009	0,093	0,005	0,002	0,047	292,1	0,023	0,247	0,280	0,349	0,049	0,06
SEY04(2)	cpx7	IG	0,001	0,006	0,808	0,007	0,095	0,019	0,006	0,069	292,5	0,022	0,249	0,350	0,418	0,064	0,06
SEY04(2)	cpx8	IG	0,000	0,002	0,515	0,004	0,062	0,006	0,003	0,042	269,5	0,024	0,274	0,321	0,390	0,060	0,05
SEY04(2)	cpx10	Gc	0,001	0,002	0,814	0,001	0,086	0,010	0,005	0,056	284,6	0,030	0,245	0,295	0,455	0,064	0,07
SEY04(2)	cpx11	Gc	0,000	0,001	0,490	0,003	0,096	0,011	0,006	0,069	277,3	0,027	0,287	0,328	0,435	0,068	0,08
SEY04(2)	cpx12	Pc	0,000	0,001	0,495	0,003	0,097	0,011	0,006	0,069	280,0	0,027	0,290	0,331	0,439	0,069	0,05
SEY04(2)	cpx12	Pr	0,000	0,002	1,085	0,006	0,081	0,007	0,004	0,114	392,5	0,031	0,328	0,426	0,395	0,073	0,07
SEY21	cpx1	SLVc	0,007	0,012	0,500	0,002	0,141	0,012	0,002	0,033	526,4	0,015	0,162	0,188	0,249	0,046	0,31
SEY21	cpx2	S	0,004	0,008	0,116	0,002		0,087	0,000	0,041	564,2	0,013	0,156	0,226	0,271	0,048	0,28
SEY22	cpx1	SLVc	0,005	0,017	0,326	0,012	0,093	0,017	0,003	0,046	392,3	0,022	0,244	0,306	0,357	0,045	0,18
SEY22	cpx2	S	0,009	0,022	0,742	0,018	0,088	0,004	0,000	0,051	379,4	0,021	0,247	0,319	0,348	0,051	0,18
SEY22	cpx2	S	0,031	0,038	0,948	0,015	0,080	0,004	0,001	0,036	393,7	0,016	0,193	0,253	0,322	0,050	0,18
SEY23(1)	cpx3	SLVc	0,029	0,081	0,490	0,019	0,479	0,022	0,017	0,167	596,6	0,043	0,333	0,312	0,319	0,040	0,49
SEY23(1)	cpx4	SLVc	0,024	0,016	0,576	0,012	0,480	0,029	0,020	0,179	569,4	0,054	0,407	0,297	0,300	0,052	0,54
SEY23(1)	cpx5	SLVc	0,019	0,017	0,485	0,009	0,361	0,026	0,014	0,161	494,8	0,038	0,290	0,206	0,225	0,033	0,56
SEY23(1)	cpx6	SLVr	0,021	0,017	0,489	0,015	0,480	0,033	0,023	0,210	587,8	0,050	0,369	0,279	0,281	0,046	0,53
SEY23(2)	cpx1	IGc	0,004	0,006	0,413	0,009	0,381	0,022	0,017	0,162	583,0	0,040	0,335	0,211	0,228	0,040	0,50
SEY23(2)	cpx2	IGr	0,011	0,016	0,659	0,008	0,338	0,021	0,014	0,131	605,6	0,039	0,276	0,239	0,217	0,038	0,46
SEY23(2)	cpx3	SLVc	0,008	0,010	0,769	0,011	0,384	0,029	0,016	0,163	579,0	0,042	0,311	0,226	0,232	0,039	0,43
SEY25	cpxA1	IGc	2,281	8,083	0,375	3,119	0,611	0,394	0,046	0,377	553,8	0,062	0,325	0,247	0,289	0,039	0,52
SEY25	cpxA2	IGc	1,220	3,450	0,469	0,768	0,387	0,096	0,031	0,182	568,8	0,038	0,334	0,232	0,248	0,039	0,54
SEY25	cpxB3	S	5,834	29,147	0,532	19,719	4,426	3,843	0,091	2,862	559,2	0,409	1,829	0,610	0,429	0,065	0,47
SEY25	cpxB4	S	4,964	23,447	0,573	13,113	2,255	2,164	0,093	1,694	692,0	0,249	1,069	0,498	0,330	0,045	0,44

The number in parentheses after sample numbers in the first column corresponds to thin section number, when two sections were analyzed in same sample. Clinopyroxene textural type: Pc and Pr, coarse (≥ 3 mm) grains in lherzolite sample, core and rim; Gc and Gr, medium (~1-2 mm) grains, core and rim; IGc and IGr, interstitial grains, core and rim; SLVc and SLVr, selvages on orthopyroxenes, core and rim; S, in S1 symplectites; F, filling cracks.